NASA TN D-1794

42p

TECHNICAL NOTE

D-1794

A STUDY OF SEVERAL FACTORS AFFECTING THE FLUTTER CHARACTERISTICS CALCULATED FOR TWO SWEPT WINGS BY PISTON THEORY AND BY QUASI-STEADY SECOND-ORDER THEORY AND COMPARISON WITH EXPERIMENTS

By Robert M. Bennett and E. Carson Yates, Jr.

Langley Research Center
Langley Station, Hampton, Va.

NATIONAL AERONAUTICS AND SPACE ADMINISTRATION

WASHINGTON May 1963

Code-1

NATIONAL AERONAUTICS AND SPACE ADMINISTRATION

TECHNICAL NOTE D-1794

A STUDY OF SEVERAL FACTORS AFFECTING THE FLUTTER CHARACTERISTICS CALCULATED FOR TWO SWEPT WINGS BY PISTON THEORY AND BY QUASI-STEADY SECOND-ORDER THEORY AND COMPARISON WITH EXPERIMENTS

By Robert M. Bennett and E. Carson Yates, Jr.

SUMMARY

The flutter characteristics of two untapered wings, one having 15° of sweepback and an aspect ratio of 5.34 and the other having 30° of sweepback and an aspect ratio of 4.16, have been investigated analytically for Mach numbers up to 3.0. The calculations employed piston theory or quasi-steady second-order theory and included variations in the number and type of vibration modes employed (i.e., measured natural modes or uncoupled beam-type modes) and in the treatment of finite wing thickness and of loading in the tip region. Results of the analysis and comparison with experiments indicated that the accuracy of flutter speeds predicted by piston theory and by quasi-steady second-order theory varied considerably, depending on several factors such as the number and type of vibration modes employed (coupled or uncoupled) and on the treatment of the aerodynamic loading near the streamwise wing tips. Best results for the two wings were not obtained by the same combination of these factors.

INTRODUCTION

In numerous flutter analyses for high supersonic Mach numbers, piston theory (refs. 1 and 2) or quasi-steady second-order theory (refs. 3 and 4) has been employed for the calculation of the required oscillatory aerodynamic forces. The pressure expressions resulting from these two theories are simple to evaluate and are well suited for flutter-trend studies and theoretical comparisons at very high Mach numbers. Many of the applications, however, have been for theoretical trend studies of two-dimensional wing sections (for example, refs. 5 to 7) or for comparisons with other flutter analyses (for example, refs. 8 and 9). On the other hand, comparisons with experimental flutter data for swept wings of finite span at moderate supersonic Mach numbers do not appear to be extensive, although some results are shown in references 4 and 10. In the flutter analysis of finite wing planforms, the effects and interactions of several pertinent factors require further examination. These factors include Mach number, leading-edge sweep, finite airfoil thickness, loading near wing tips, and number and type of vibration modes.

The influences of these factors on flutter characteristics calculated by second-order piston theory and by quasi-steady second-order theory are investigated herein for two homogeneous untapered swept wings at Mach numbers from 1.65 to 3.00. The results are compared with the experimental flutter data of reference 11. Flutter calculations were made both with and without consideration of finite wing thickness. In these calculations three different methods were used for evaluating the aerodynamic loading within the triangular region affected by the streamwise wing tips. The calculations were performed with two or three natural (coupled) vibration modes or with two, three, or four uncoupled vibration modes.

SYMBOLS

b_s semichord measured streamwise

k reduced frequency, $\frac{b_s \omega}{V}$

M Mach number

$\bar{m}$ total mass of wing panel

Δp lifting pressure

t time

V flutter speed

v volume of air within a cylinder having the streamwise chord as base diameter and the panel span as height

$\bar{x}$ streamwise distance measured rearward from wing leading edge, fraction of local chord

$\bar{y}$ spanwise distance measured from wing root, fraction of panel span

$\bar{Z}$ magnitude of airfoil ordinate measured normal to chord plane, fraction of local chord

$\bar{z}$ amplitude of vertical displacement at point $(\bar{x},\bar{y})$ on wing panel

z_k modal deflection for k^{th} coupled vibration mode

$z_{h,i}$ modal deflection for i^{th} uncoupled bending vibration mode

$z_{\alpha,j}$ modal deflection for j^{th} uncoupled torsional vibration mode

$\beta = \sqrt{M^2 - 1}$

γ ratio of specific heats

Λ sweep angle

$\bar{\mu}$ mass ratio for wing panel, $\frac{\bar{m}}{\rho v}$

ρ air density

ω circular frequency of vibration at flutter

ω_k circular frequency of k^{th} coupled vibration mode

$\omega_{h,i}$ circular frequency of i^{th} uncoupled bending vibration mode

$\omega_{\alpha,j}$ circular frequency of j^{th} uncoupled torsional vibration mode

WINGS

General Description

The flutter calculations of this report were made for two of the untapered, swept wings for which experimental flutter data were given in reference 11. One wing was swept back 15° and had an aspect ratio of 5.34; the other wing was swept back 30° and had an aspect ratio of 4.16. (See fig. 1.) These wings were cut from 0.041-inch-thick magnesium sheet, and had chords of 2 inches measured perpendicular to the leading edge. As shown in figure 1, the leading and trailing edges of both wings were beveled 1/4 inch to form a 2.05-percent-thick symmetrical hexagonal airfoil section perpendicular to the leading edge. For these homogeneous untapered wings, both the elastic axis and the local centers of gravity were taken to be at midchord.

In the investigation of reference 11, two magnesium models and two aluminum models of each planform were flutter tested. For convenient reference, the models that were tested at supersonic speeds are designated as A, B, and C. Flutter calculations are presented herein only for 15° wing models A and B, and for 30° wing models A and B (see table I), although experimental flutter data for 15° and 30° wing models C are included to indicate the experimental trends.

These wings seemed particularly appropriate for this investigation for several reasons:

(1) Because of the sharp leading edges and relatively small sweep angles, piston theory and quasi-steady second-order theory should be reasonably accurate at fairly low supersonic Mach numbers.

(2) The large streamwise tips should have a sizable effect on the aerodynamic loading.

(3) Some of the measured natural vibration modes for these wings (ref. 12) indicate a high degree of bending-torsion coupling so that coupled-mode and

uncoupled-mode representations of these wings should provide quite different inputs to the flutter analysis.

(4) Experimental flutter data (ref. 11) were available for comparison.

Mode Shapes and Frequencies

The first three natural (coupled) mode shapes for both wings were measured by a bouncing sand technique. The resulting deflections were presented in reference 12 and are repeated for convenience herein in figures 2(a) and 3(a). The corresponding measured coupled-mode frequencies for the models of this investigation were given with the flutter test data in reference 11, and are summarized in table I of the present report. The node lines for these wings (fig. 1) indicate that the second and third natural modes involve a high degree of bending-torsion coupling, particularly for the 30° wing.

Since the wings employed herein were homogeneous and untapered, the uncoupled mode shapes and frequencies for both planforms were considered to be the same as those for a uniform cantilever beam. The use of uncoupled modes implies that wing sections normal to the elastic axis (midchord for the present two wings) are considered to oscillate without distortion. For swept wings, these sections do not lie in the free-stream direction, so that some camber of streamwise sections appears (figs. 2(b) and 3(b)) as it does in the measured coupled modes. The first three bending-mode and first torsion-mode frequencies for 15° wing models A and C and the first two bending-mode and first two torsion-mode frequencies for 30° wing models A and C were calculated from the simple formulas for a uniform cantilever beam. To allow for slight differences in stiffness between ostensibly identical models A and B, the uncoupled-mode frequencies for model B were obtained from those for model A by multiplying by the ratio of the measured first-mode frequency of model B to the corresponding frequency of model A; that is, for models B of both planforms,

$$\left(\omega_{h,i}\right)_B = \frac{\left(\omega_1\right)_B}{\left(\omega_1\right)_A} \times \left(\omega_{h,i}\right)_A$$

and

$$\left(\omega_{\alpha,j}\right)_B = \frac{\left(\omega_1\right)_B}{\left(\omega_1\right)_A} \times \left(\omega_{\alpha,j}\right)_A$$

The uncoupled-mode frequencies for all models are presented in table I. For each model, the frequency of the second bending mode is close to that of the first torsion mode, and both are near the measured second- and third-mode natural (coupled) frequencies.

FLUTTER CALCULATIONS

The aerodynamic forces for the present flutter calculations were based on the expressions for lifting pressure given in reference 4 for second-order piston theory and for quasi-steady second-order theory. The quasi-steady second-order theory employed herein and in reference 4 is based on the steady-flow second-order theory of reference 3 and should not be confused with the unsteady second-order theory of reference 13. The quasi-steady theory was used here because the measured reduced frequencies at flutter for the present wings were small (table I) and because the calculations could be made with the same computing program used for the piston-theory calculations. Accordingly, for harmonic motion the expressions for lifting pressure may be written as

$$\frac{\Delta p(\bar{x},\bar{y},t)}{\rho V^2/2} = \frac{4}{M}\left[1 + M\,\frac{\gamma+1}{2}\,\frac{\partial \bar{Z}(\bar{x},\bar{y})}{\partial \bar{x}}\right]\left[\left(\frac{\partial}{\partial \bar{x}} + ik\right)\bar{z}(\bar{x},\bar{y})\right] e^{i\omega t} \tag{1}$$

for piston theory and as

$$\frac{\Delta p(\bar{x},\bar{y},t)}{\rho V^2/2} = \frac{4}{\beta}\left[1 + \frac{M^4(\gamma+1) - 4\beta^2}{2\beta^3}\,\frac{\partial \bar{Z}(\bar{x},\bar{y})}{\partial \bar{x}}\right]\left[\left(\frac{\partial}{\partial \bar{x}} + ik\right)\bar{z}(\bar{x},\bar{y})\right] e^{i\omega t} \tag{2}$$

for quasi-steady second-order theory. These lifting-pressure expressions are similar in form, with second-order theory differing from piston theory only in two coefficients that are functions only of Mach number and the ratio of specific heats. Both theories permit the inclusion of airfoil shape and coupled vibration modes with camber.

In the quasi-steady theory (ref. 4) the pressure expression in equation (2) is used to represent the pressure distribution on an oscillating wing as though it were composed of a succession of steady-state distributions each associated with an instantaneous angle of attack. This procedure is reasonable for high Mach numbers because the reduced frequency at flutter generally decreases as Mach number increases. Thus, at high Mach numbers the unsteady aspects of the flow have reduced significance.

Most of the flutter calculations for the wings of this report included the effect of finite wing thickness and employed the first three coupled vibration modes or three uncoupled modes (first and second bending and first torsion). Some additional calculations for both wings neglected finite wing thickness, and some employed only the first two coupled modes or two uncoupled modes (first bending and first torsion) for comparison purposes[1]. (See table II.) The fourth

[1]In view of the closeness of the second and third natural frequencies and of the first torsion and second bending frequencies for these two wings (table I) and in view of the high degree of bending-torsion coupling shown in both the second and third natural modes (ref. 12), the use of at least three vibration modes would ordinarily be indicated for flutter analysis of these wings. The two-mode calculations included herein are therefore considered to be of analytical interest only.

uncoupled mode (third bending for the 15° swept wing, second torsion for the 30° swept wing) was included in some uncoupled-mode calculations in order to indicate the degree of convergence of the present modal representations. The coupled modes were not assumed orthogonal, and the off-diagonal generalized masses, though small, were included in the flutter determinant. For the uncoupled-mode calculations, however, the off-diagonal generalized masses were identically zero. Since the pertinent structural damping values are not known for the models used in this investigation, and since the damping coefficients for cantilevered solid metal wings of the present type are usually very small, all calculated flutter points herein are taken to be points for which the required structural damping vanishes. All integrations required for the evaluation of the generalized aerodynamic forces and of the generalized masses were performed by use of an 11-point Simpson's rule.

Piston theory and quasi-steady second-order theory as expressed in reference 4 take no account of streamwise wing tips. However, for some of the calculations of this report and of reference 14, an approximate tip-load modification was made on the basis of steady-flow linear theory. The streamwise tip, of course, influences loading only within the triangular region bounded by the tip, the trailing edge, and the Mach line from the leading-edge tip; and the area of this triangle decreases as Mach number increases. Furthermore, the reduced frequency at flutter generally decreases as Mach number increases so that a steady-flow type of tip-load modification should be more accurate at the higher Mach numbers. The tip-load modification as applied herein and in reference 14 consists of multiplying the piston-theory or second-order-theory loading at each point within the tip triangle by the ratio of steady-state load with streamwise tip to steady-state load without streamwise tip. This ratio, of course, varies with the location of the point within the tip triangle and with Mach number. Thus for piston theory, for example, the corrected lifting pressure at a point $(\bar{x},\bar{y})$ on the wing is given by

$$\Delta p(\bar{x},\bar{y},M)_{\text{piston theory corrected}} = \Delta p(\bar{x},\bar{y},M)_{\text{piston theory uncorrected}} \times \frac{\Delta p(\bar{x},\bar{y},M)_{\text{linear theory with tip}}}{\Delta p(\bar{x},\bar{y},M)_{\text{linear theory without tip}}} \quad (3)$$

Such calculations for the wings of this report should give an indication of the merit of this modification because these wings were untapered and of moderate aspect ratio so that the tip triangle included a sizable portion of the wing area at the lower Mach numbers. The sensitivity of the calculations to this modification was examined by computing flutter characteristics for the 15° wing with no tip-load modification, with the above-mentioned tip-load modification, and with zero load assumed within the tip triangle. (See table II.) The first and last of these procedures represent limiting cases. For the 30° wing, either no tip-load modification or the calculated modification was used.

PRESENTATION OF RESULTS

A summary of pertinent conditions for all the calculations and an index to the results are provided in table II. In figures 4 to 15 the supersonic flutter speeds and frequencies calculated for the 15° and 30° wings by piston theory and by quasi-steady second-order theory are compared with the flutter experiments of reference 11. Figures 4 to 7 and 10 to 13 show the effects on the calculated flutter characteristics of the number and type of vibration modes employed and of the inclusion of finite wing thickness. Figures 8 and 9, together with figures 10, 11, 14, and 15, present the results obtained with the three different representations of loading in the tip region.

DISCUSSION OF RESULTS

In the calculations of all the flutter-speed and flutter-frequency curves of figures 4 to 15, the wing properties and flow density employed were those associated with the experimental flutter points shown. Since each experimental point (from ref. 11) represents a different model and a different density, the calculations for each model and density were limited to a range of Mach number which bracketed the experimental value. Specifically, the Mach numbers covered are 2.50 to 3.00 for model A and 1.65 to 2.50 for model B. Because of the discontinuous change of mass ratio and modal frequencies, the calculated flutter characteristics show discontinuities at $M = 2.50$.

Figures 4 to 15 indicate that for the present two wings the closest agreement between theory and experiment was not attained with the same combination of the variable factors (i.e., piston theory or quasi-steady second-order theory, number and type of vibration modes, wing thickness, and tip-load modification). Furthermore, the effects of varying these factors were frequently different for the two wings. The subsequent sections of this report discuss the results obtained by changing each of these factors individually.

Comparison of Results From Piston Theory and From Quasi-Steady Second-Order Theory

The flutter speeds calculated for these wings from quasi-steady second-order theory were lower than those calculated from piston theory. In addition to being lower, the flutter-speed coefficients calculated by second-order theory generally followed the experimental trend of flutter-speed coefficient with Mach number more closely, particularly at the lower supersonic Mach numbers. Furthermore, there was usually little difference between the flutter frequencies obtained from these two theories. Since the lifting-pressure expressions associated with piston theory and with quasi-steady second-order theory (ref. 4) approach each other as Mach number approaches infinity, the flutter speeds indicated by the two theories also approach each other as Mach number increases. In view of these statements, the following discussion is concerned with the results of the second-order-theory calculations unless otherwise specified.

Results for 15° Wing

Number and type of vibration modes.- For the 15° wing, results of the flutter calculations which include two, three, or four uncoupled vibration modes, finite wing thickness, and no modification of aerodynamic loading in the tip region are shown in figures 4(a) and 5(a). For all Mach numbers the calculated flutter-speed coefficients decrease as the number of uncoupled modes is increased. However, the difference between three-mode and four-mode calculations is insignificant except at the lowest Mach numbers where the four-mode piston-theory calculation produced two flutter solutions which indicated that flutter could occur in either of two modes. Only the solution yielding the lower flutter speed is shown in figures 4(a) and 5(a). The corresponding second-order-theory calculations indicated the possibility of a similar double solution at Mach numbers lower than those calculated.

Figures 4(b) and 5(b) present flutter characteristics for the 15° wing calculated with two or three coupled vibration modes, finite wing thickness, and no tip-load modification. In contrast to the results with uncoupled modes, the addition of the third coupled mode increases the calculated flutter speed at all Mach numbers. Since higher coupled modes are not available from the measurements of reference 12, it is not known whether their inclusion in the flutter calculations would lead to further changes in the results.

The flutter speeds calculated with three coupled modes (fig. 4(b)) are lower than those calculated with three uncoupled modes (fig. 4(a)). (See also fig. 8(a).) For all Mach numbers, however, the difference is less than 10 percent. For these two calculations, the agreement with experiment is satisfactory at Mach number 3.0, but becomes poorer as Mach number decreases.

The calculated flutter frequency ratios (figs.5(a) and (b)) are in satisfactory agreement with experiment and generally show little change as the number of vibration modes is increased.

Calculations similar to those represented in figures 4 and 5 but without finite wing thickness yield the flutter speeds and frequencies shown in figures 6 and 7. Inclusion of the third uncoupled mode (fig. 6(a)) depresses the calculated flutter speed, whereas inclusion of the third coupled mode (fig. 6(b)) raises the flutter speed. This result indicates changes that are in the same direction as when thickness is included. The magnitudes of the changes in figure 6 (thickness neglected) are much greater than those in figure 4 (thickness included). For example, the two-uncoupled-mode calculation gave no solution when thickness was omitted.

Wing thickness.- Flutter calculations employing two uncoupled vibration modes yield finite flutter speeds when finite wing thickness is included (fig. 4(a)), but not when thickness is neglected. Hence, in this case the effect of thickness is large and destabilizing. This behavior is in qualitative agreement with the results of two-dimensional piston-theory calculations for low ratios of bending frequency to torsion frequency (refs. 5 and 7 to 9). In reference 15 flutter experiments and representative-section piston-theory calculations for a wing of rectangular planform also showed a destabilizing effect of thickness. In contrast

to these results, the omission of finite wing thickness in three-uncoupled-mode calculations is destabilizing and yields conservative flutter speeds. (Compare figs. 4(a) and 6(a).) The binary flutter trends for two-dimensional wings in figure 2 of reference 9 and in figure 13 of reference 7 also show that the inclusion of finite thickness can be stabilizing in some cases. The appreciable difference in levels of flutter-speed coefficient between models A and B (see fig. 6(a) at M = 2.50) is caused entirely by the difference in flow density shown in table I; thus, for these conditions the calculated flutter dynamic pressure is not invariant with changes in density.

The inclusion of finite thickness in flutter calculations with two coupled vibration modes (compare fig. 4(b) and 6(b)) has a destabilizing effect that is small in comparison with that indicated by the calculations with two uncoupled modes even though the modal-frequency ratios are small in both cases. On the other hand, in the calculations with three coupled modes, inclusion of thickness has large depressing effects on both flutter speed and frequency. (See figs. 4(b), 5(b), 6(b), and 7(b).) Similar calculations with three coupled modes for an untapered 45° swept wing (ref. 4) showed little effect of wing thickness. Since the airfoil (normal to the leading edge) for this 45° swept wing was the same as that for the present 15° and 30° wings, the thickness ratio and contour slopes in the streamwise direction were lower for the wing of reference 4. Further indications of the influence of wing thickness and other parameters on representative-section piston-theory flutter trends are presented, for example, in references 5 to 8.

It is evident from figures 6(b) and 7(b) that the calculations with three coupled modes and no thickness are far more sensitive to changes in flow density and modal-frequency ratios than are any of the previously mentioned calculations. At M = 2.50, the only quantities differing in the coupled-mode calculations for models A and B are the flow density and the ratio of second-mode to third-mode frequency. (See table I(a).) Some further discussions of the effects of flow density are included in references 14 and 16.

Load representation in the tip region.- Progressive reduction of the aerodynamic loading in the triangular region influenced by the tip from the no-tip-modification level to the calculated tip-modification level and then to the zero-load condition is shown in figures 8 and 9 to cause progressive reduction in the calculated flutter-speed coefficients and flutter frequency ratios. Furthermore, the use of the calculated tip-load modification (calculated from steady-flow theory as previously described) reduces the calculated flutter speed more at lower Mach numbers than at higher Mach numbers. (Compare figs. 8(a) and 8(b).) Hence, when the calculated tip-load modification is employed, the slope of the curve of flutter-speed coefficient against Mach number (fig. 8(b)) increases and corresponds more closely to the experimental trend. In comparison, the limiting case of zero load in the tip region (fig. 8(c)) gives still lower flutter speeds, but the trends appear increasingly conservative as Mach number increases. In all cases, the lowest flutter speeds and frequencies are obtained from quasi-steady second-order theory with coupled vibration modes. In contrast, in similar calculations for the highly tapered 45° swept wing of reference 14, the lowest flutter speeds were obtained from the second-order theory with uncoupled vibration modes. However, use of the calculated tip-load modification in reference 14 lowered the calculated flutter speed as in the present case.

Best results.- For the 15° wing, the best overall predictions of flutter-speed trends and magnitudes were obtained from quasi-steady second-order-theory calculations in which finite wing thickness was included and in which coupled vibration modes and the calculated tip-load modification were employed (fig. 8(b)). Even for this calculation the predicted flutter speed at $M = 2.00$ is unconservative by about 10 percent. For comparison, the rule of thumb given in reference 5 for the applicability of piston theory, namely that $M \cos \Lambda \geq 2.5$, is satisfied for the 15° wing only for $M \geq 2.6$. Above this Mach number the agreement between the present best results and experiment appears to be very good.

Results for 30° Wing

Number and type of vibration modes.- For the 30° wing, results of the flutter calculations which include two, three, or four uncoupled vibration modes, finite wing thickness, and no modification of aerodynamic loading in the tip region are shown in figures 10 and 11. The flutter-speed coefficients and flutter frequency ratios calculated with two modes are excessively high and no flutter solutions occurred for $M \leq 2.40$. In contrast, inclusion of the second bending mode yields flutter speeds that are slightly conservative and in good agreement with experimental values, although the calculated flutter frequencies remain high. Thus, the second bending mode has a much more significant effect on the flutter results for the 30° wing than for the 15° wing. (Compare figs. 4(a) and 10 and figs. 5(a) and 11.) As in the case of the 15° wing, the inclusion of the fourth uncoupled mode, which for the 30° wing is the second torsion mode, gives flutter speeds and frequencies which are essentially the same as the three-mode values.

When finite wing thickness is neglected (figs. 12 and 13), the results for the 30° wing are qualitatively the same as for the 15° wing (figs. 6(a) and 7(a)). That is, no flutter solution occurred when two modes were used, whereas the flutter speeds obtained with three modes were excessively conservative.

Similar calculations employing two or three coupled vibration modes, with or without finite wing thickness and without the tip-load modification, gave no flutter solution. In contrast, similar calculations for the 15° wing of the present report and for the untapered 45° wing of reference 4 yielded finite flutter speeds and frequencies. The calculated flutter speeds for the wing of reference 4, however, were unconservative, and the calculated flutter frequencies were nearly twice the experimental values.

Wing thickness.- Figures 10 and 12 indicate that when uncoupled vibration modes are employed, changes in the calculated flutter speed caused by the inclusion of wing thickness are in the same direction as those shown previously for the 15° wing. In the two-mode calculations, flutter solutions occurred only at the higher Mach numbers and only when thickness was included. Therefore, the effect of thickness was large and destabilizing, at least at these higher Mach numbers. The inclusion of thickness in the three-mode calculations again was stabilizing, particularly at the higher Mach numbers.

Load representation in the tip region.- Comparisons of figures 10 and 14 and figures 11 and 15 show the effects of employing the calculated modification to the

aerodynamic loading in the tip region for the calculations with three vibration modes and with finite thickness. For the 30° wing, no calculations were made for the limiting condition of zero load in the tip region. At the higher Mach numbers, the uncoupled-mode calculations for the 30° wing show that use of the calculated tip-load modification causes a moderate reduction in flutter speed as it did in the case of the 15° wing. At Mach numbers near 2.00, however, the tip-load modification has little effect, and at the lowest Mach numbers it even increases the calculated flutter speed (figs. 10 and 14). These varying effects of the tip-load modification with Mach number may be related to two predominant influences which the modification has in the flutter analyses. First, application of the calculated tip-load modification reduces the magnitude of the aerodynamic loading in the tip triangle; this reduction would tend to increase the calculated flutter speed. Second, use of the tip-load modification shifts the center of loading forward in the tip region; this shift generally tends to decrease the calculated flutter speed. Apparently, for the 30° wing, the former effect dominates at the lower Mach numbers, and the latter effect dominates at the higher Mach numbers. In calculations employing uncoupled vibration modes, use of the tip-load modification caused negligible change in the calculated flutter frequencies which remain considerably higher than experimental values (fig. 15).

Although no coupled-mode flutter solution was obtained without the tip-load modification, use of the modification in coupled-mode flutter calculations yielded finite flutter speeds; however, these results are unconservative and are not in good agreement with experiment (fig. 14). The corresponding calculated flutter frequencies are in fair agreement with experiment (fig. 15). These results indicate that coupled-mode calculations for the 30° wing are highly sensitive to the treatment of the loading in the tip region.

Best results.- For the 30° wing, the combination of factors yielding the best calculated flutter characteristics is not as clearly defined as for the 15° wing. Piston-theory and quasi-steady second-order-theory flutter calculations employing three uncoupled vibration modes and finite wing thickness, with or without the calculated tip-load modification, give flutter speeds that are close together and moderately conservative at all but the lowest Mach numbers. Since these flutter speeds are conservative and since the values given by piston theory are slightly higher than those given by the quasi-steady second-order theory, the piston-theory values are slightly closer to the experimental points. On the other hand, more accurate values of flutter frequency are obtained from the second-order theory with three coupled modes, finite thickness, and the calculated tip-load modification (fig. 14), although the corresponding flutter speed is about 50 percent high at $M = 2.00$. The rule of thumb for the applicability of piston theory (ref. 5), namely that $M \cos \Lambda \geqq 2.5$, is satisfied for the 30° wing only for $M \geqq 2.9$. In view of this criterion and the previous discussion, the most satisfactory calculations for the 30° wing are considered to be obtained from either piston theory or quasi-steady second-order theory with three uncoupled vibration modes, finite wing thickness, and no tip-load modification.

CONCLUDING REMARKS

The flutter characteristics of two untapered swept wings have been investigated analytically for Mach numbers up to 3.0 by piston theory and by quasi-steady second-order theory. The calculations included variations in the number and type of vibration modes employed (i.e., measured natural modes or uncoupled beam-type modes) and in the treatment of finite wing thickness and of loading in the tip region.

For the present two wings, the closest overall agreement between theory and experiment was not attained with the same combination of the previously mentioned variable factors, and the effects of varying these factors were frequently different for the two wings. For example, the best results for the 15° wing were obtained from the quasi-steady second-order theory with coupled vibration modes, finite wing thickness, and a modification of the loading near streamwise wing tips based on three-dimensional steady-flow theory. On the other hand, for the 30° wing, flutter characteristics given by piston theory and by quasi-steady second-order theory were generally close together, and best results were obtained with uncoupled vibration modes, finite wing thickness, and no modification of loading in the tip region. Furthermore, the effect of including either finite wing thickness or the calculated tip-load modification can be large or small and either stabilizing or destabilizing depending, for example, on number and type of vibration modes, modal-frequency ratios, planform, and Mach number. However, the quasi-steady second-order theory generally yielded calculated flutter speeds which were lower and in better agreement with experimental trends than those given by piston theory, particularly at the lower Mach numbers.

Langley Research Center,
National Aeronautics and Space Administration,
Langley Station, Hampton, Va., March 8, 1963.

REFERENCES

1. Lighthill, M. J.: Oscillating Airfoils at High Mach Number. Jour. Aero. Sci., vol. 20, no. 6, June 1953, pp. 402-406.

2. Ashley, Holt, and Zartarian, Garabed: Piston Theory - A New Aerodynamic Tool for the Aeroelastician. Jour. Aero. Sci., vol. 23, no. 12, Dec. 1956, pp. 1109-1118.

3. Van Dyke, Milton D.: A Study of Second-Order Supersonic Flow Theory. NACA Rep. 1081, 1952. (Supersedes NACA TN 2200.)

4. Morgan, Homer G., Huckel, Vera, and Runyan, Harry L.: Procedure for Calculating Flutter at High Supersonic Speed Including Camber Deflections, and Comparison With Experimental Results. NACA TN 4335, 1958.

5. Ashley, Holt, and Zartarian, Garabed: Supersonic Flutter Trends as Revealed by Piston Theory Calculations. WADC Tech. Rep. 58-74, ASTIA Doc. No. AD 155513, U.S. Air Force, May 1958.

6. Weatherill, Warren H., and Zartarian, Garabed: Tabular Presentation of Supersonic Flutter Trends From Piston Theory Calculations. WADC Tech. Note 57-310, ASTIA Doc. No. AD 142154, U.S. Air Force, Jan. 1958.

7. Chawla, Jagannath P.: Aeroelastic Instability at High Mach Number. Jour. Aero. Sci., vol. 25, no. 4, Apr. 1958, pp. 246-258.

8. Morgan, Homer G., Runyan, Harry L., and Huckel, Vera: Theoretical Considerations of Flutter at High Mach Numbers. Jour. Aero. Sci., vol. 25, no. 6, June 1958, pp. 371-381.

9. Runyan, Harry L., and Morgan, Homer G.: Flutter at Very High Speeds. NASA TN D-942, 1962. (Supersedes NACA RM L57D16a.)

10. Morgan, Homer G., Figge, Irving E., and Presnell, John G., Jr.: Investigation of Flutter Characteristics of Three Low-Aspect-Ratio All-Movable Half-Span Control Surfaces at Mach Numbers From 1.49 to 2.87. NACA RM L58B20, 1958.

11. Tuovila, W. J., and McCarty, John Locke: Experimental Flutter Results for Cantilever-Wing Models at Mach Numbers up to 3.0. NACA RM L55E11, 1955.

12. Hanson, Perry W., and Tuovila, W. J.: Experimentally Determined Natural Vibration Modes of Some Cantilever-Wing Flutter Models by Using an Acceleration Method. NACA TN 4010, 1957.

13. Van Dyke, Milton D.: Supersonic Flow Past Oscillating Airfoils Including Nonlinear Thickness Effects. NACA Rep. 1183, 1954. (Supersedes NACA TN 2982.)

14. Yates, E. Carson, Jr.: Subsonic and Supersonic Flutter Analysis of a Highly Tapered Swept-Wing Planform, Including Effects of Density Variation and Finite Wing Thickness, and Comparison With Experiments. NASA TM X-764, 1963.

15. Martucelli, John R.: Flutter Model Tests at Mach Numbers 1.5-5.0. WADC Tech. Rep. 59-407, U.S. Air Force, Sept. 1959.

16. Yates, E. Carson, Jr.: Some Effects of Variations in Density and Aerodynamic Parameters on the Calculated Flutter Characteristics of Finite-Span Swept and Unswept Wings at Subsonic and Supersonic Speeds. NASA TM X-182, 1960.

TABLE I.- MODAL FREQUENCIES AND FLUTTER TEST CONDITIONS

(a) Wing with 15° sweepback

Model	Material	Coupled-mode frequencies			Uncoupled-mode frequencies				Test conditions			
		ω_1, rad/sec	ω_2, rad/sec	ω_3, rad/sec	$\omega_{h,1}$, rad/sec	$\omega_{h,2}$, rad/sec	$\omega_{h,3}$, rad/sec	$\omega_{\alpha,1}$, rad/sec	M	ρ, slug/ft^3	$\bar{\mu}$	k
A	Magnesium	232	1,370	1,696	245	1,537	4,303	1,456	3.00	0.00093	79	0.0390
B	Magnesium	220	1,288	1,470	232	1,454	4,071	1,377	2.00	.00053	139	.0432
C	Aluminum	226	1,319	1,596	251	1,575	-----	1,488	1.30	.00049	234	.0432

(b) Wing with 30° sweepback

Model	Material	Coupled-mode frequencies			Uncoupled-mode frequencies				Test conditions			
		ω_1, rad/sec	ω_2, rad/sec	ω_3, rad/sec	$\omega_{h,1}$, rad/sec	$\omega_{h,2}$, rad/sec	$\omega_{\alpha,1}$, rad/sec	$\omega_{\alpha,2}$, rad/sec	M	ρ, slug/ft^3	$\bar{\mu}$	k
A	Magnesium	264	1,351	1,866	260	1,629	1,496	4,490	3.00	0.00067	100	0.0470
B	Magnesium	239	1,319	1,640	235	1,473	1,353	4,059	2.00	.00043	156	.0511
C	Aluminum	245	1,319	1,721	267	1,673	1,533	-----	1.30	.00044	234	.0444

TABLE II.- SUMMARY OF PERTINENT CONDITIONS AND INDEX TO RESULTS OF FLUTTER CALCULATIONS

Vibration modes	Aerodynamic parameters		15° swept wing		30° swept wing	
	Finite thickness	Load in tip triangle	Results shown in figure		Results shown in figure	
			$\frac{V}{\sqrt{\bar{\mu}} b_s \omega_{\alpha,1}}$	$\frac{\omega}{\omega_{\alpha,1}}$	$\frac{V}{\sqrt{\bar{\mu}} b_s \omega_{\alpha,1}}$	$\frac{\omega}{\omega_{\alpha,1}}$
4 uncoupled	Yes	Unmodified	4(a)	5(a)	10	11
3 uncoupled	Yes	Calculated modification	8(b)	9(b)	14	15
	Yes	Zero load	8(c)	9(c)	---	---
	Yes	Unmodified	4(a), 8(a)	5(a), 9(a)	10	11
	No	Unmodified	6(a)	7(a)	12	13
2 uncoupled	Yes	Unmodified	4(a)	5(a)	10	11
	No	Unmodified	6(a)*	7(a)*	12*	13*
3 coupled	Yes	Calculated modification	8(b)	9(b)	14	15
	Yes	Zero load	8(c)	9(c)	---	---
	Yes	Unmodified	4(b), 8(a)	5(b), 9(a)	(*)	(*)
	No	Unmodified	6(b)	7(b)	(*)	(*)
2 coupled	Yes	Unmodified	4(b)	5(b)	(*)	(*)
	No	Unmodified	6(b)	7(b)	(*)	(*)

*No flutter indicated by calculations.

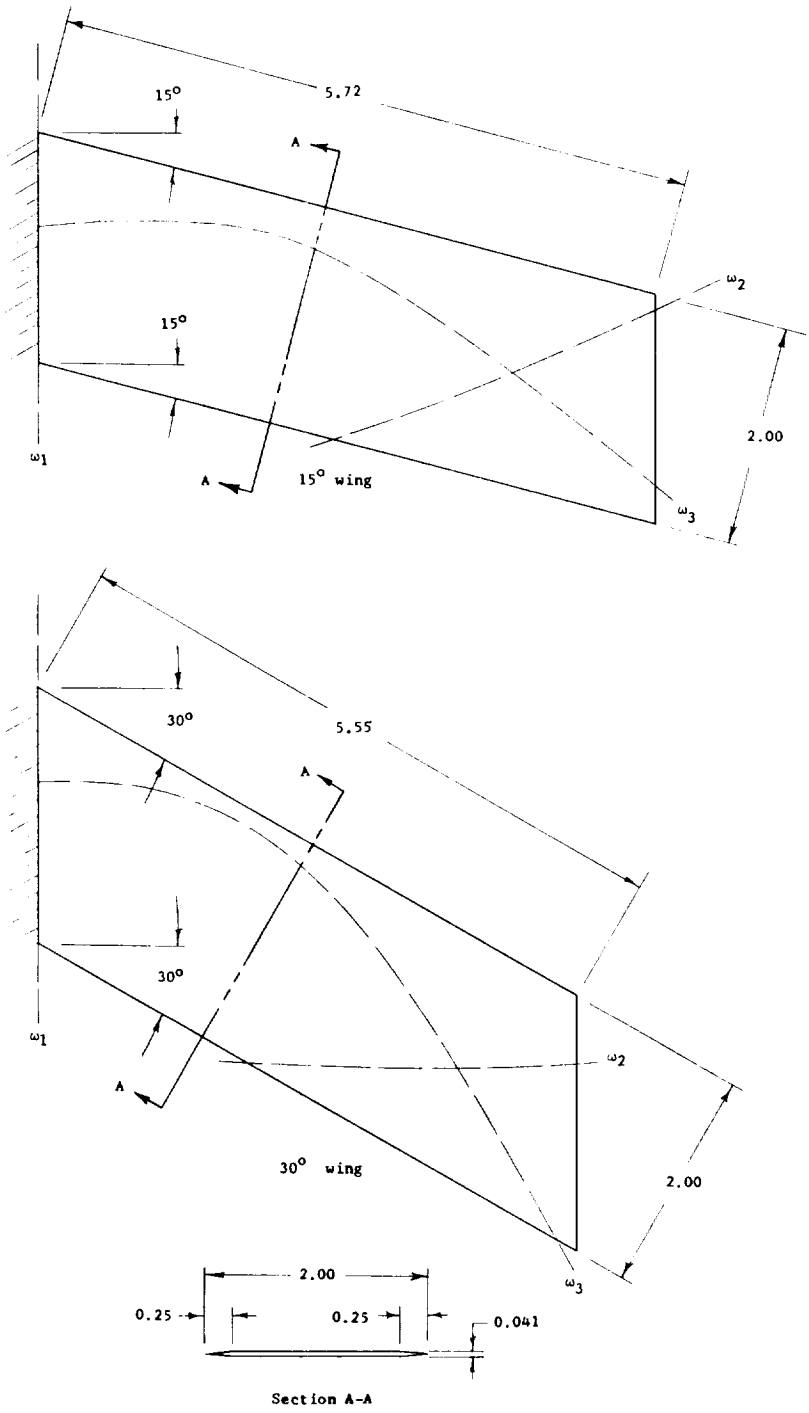

Figure 1.- Sketch of wing planforms showing measured node lines. (All dimensions are in inches unless otherwise specified.)

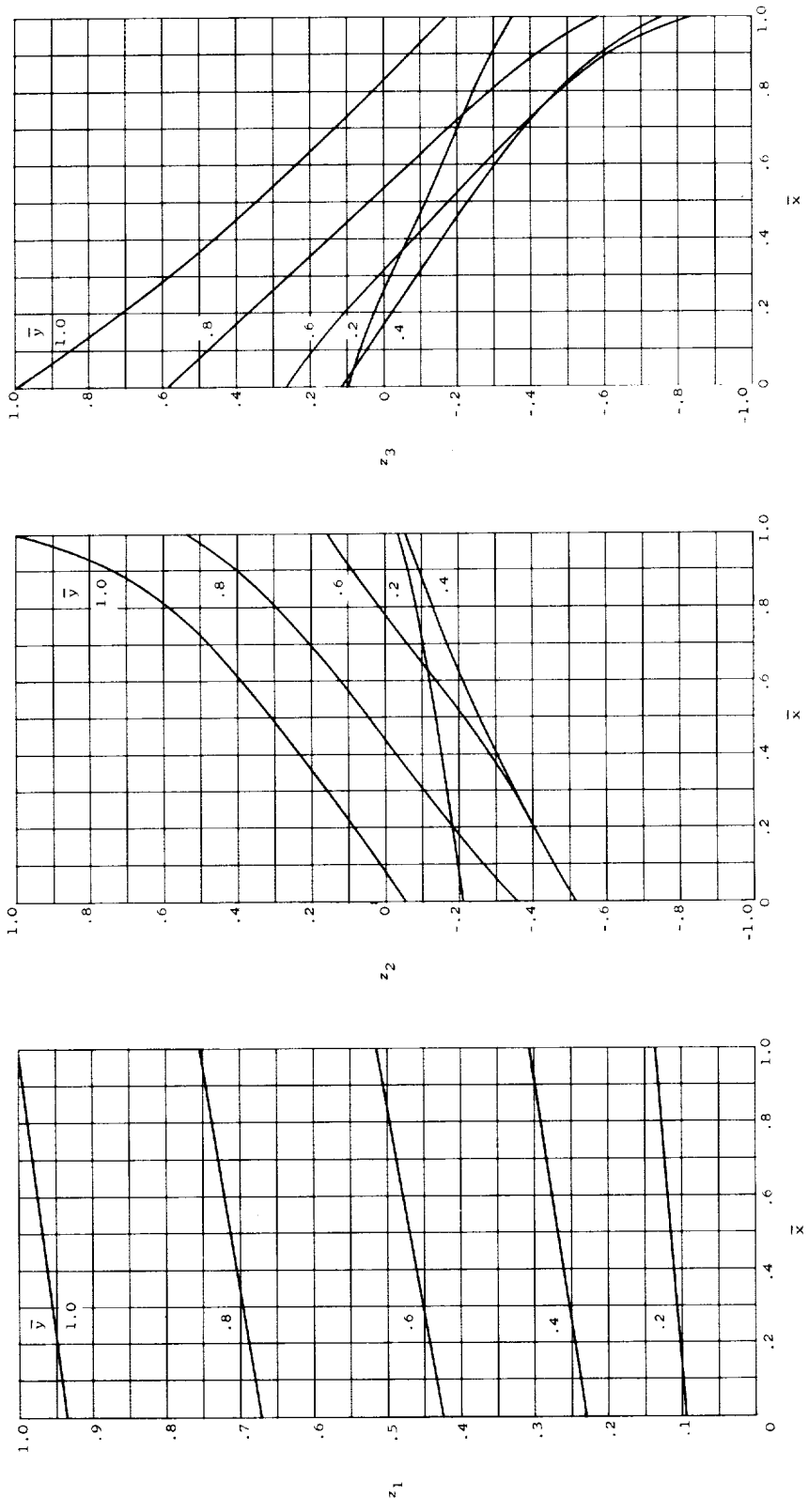

(a) Coupled modes.

Figure 2.- Vibration modes for 15° wing.

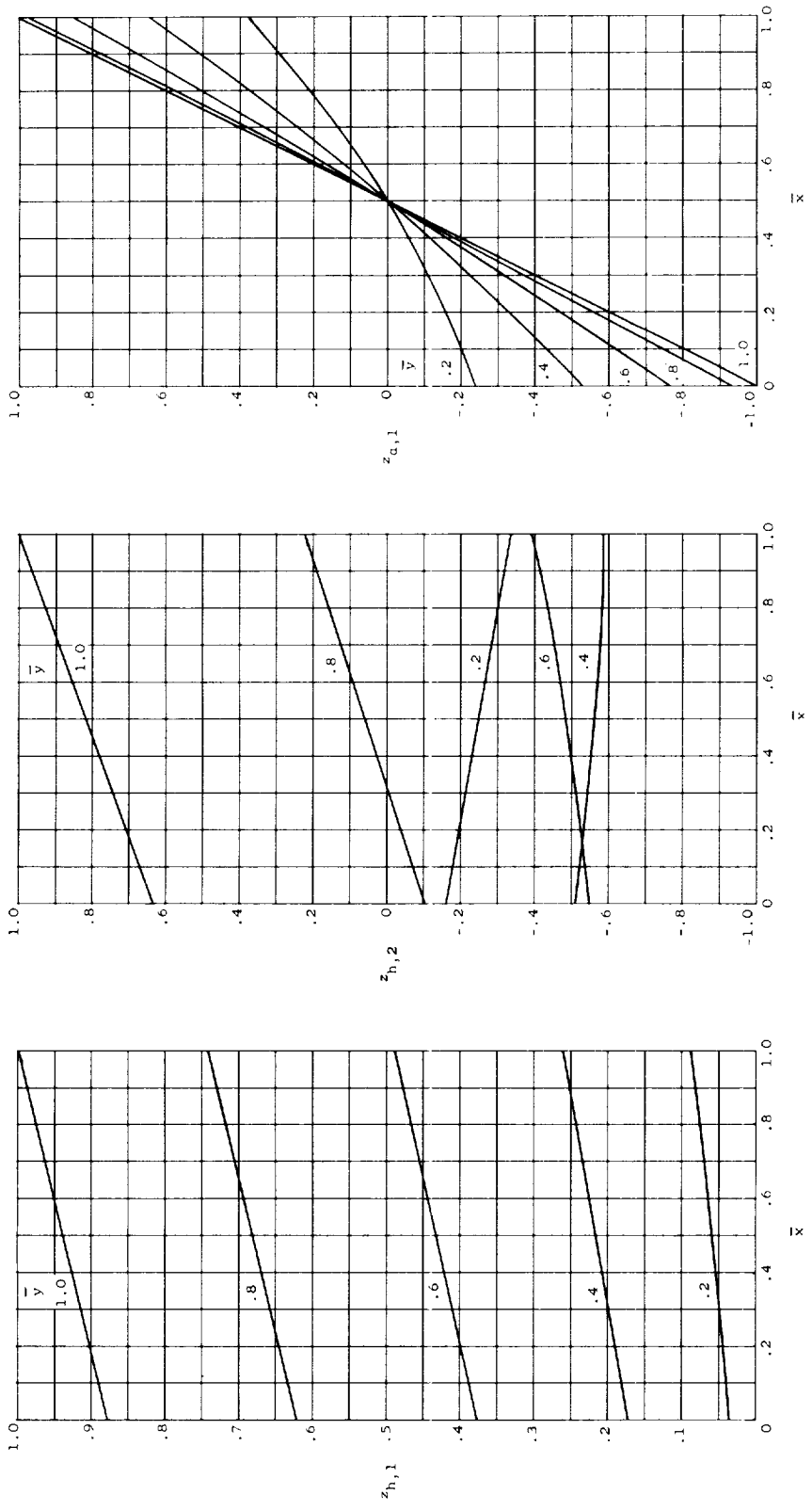

(b) Uncoupled modes.

Figure 2.- Concluded.

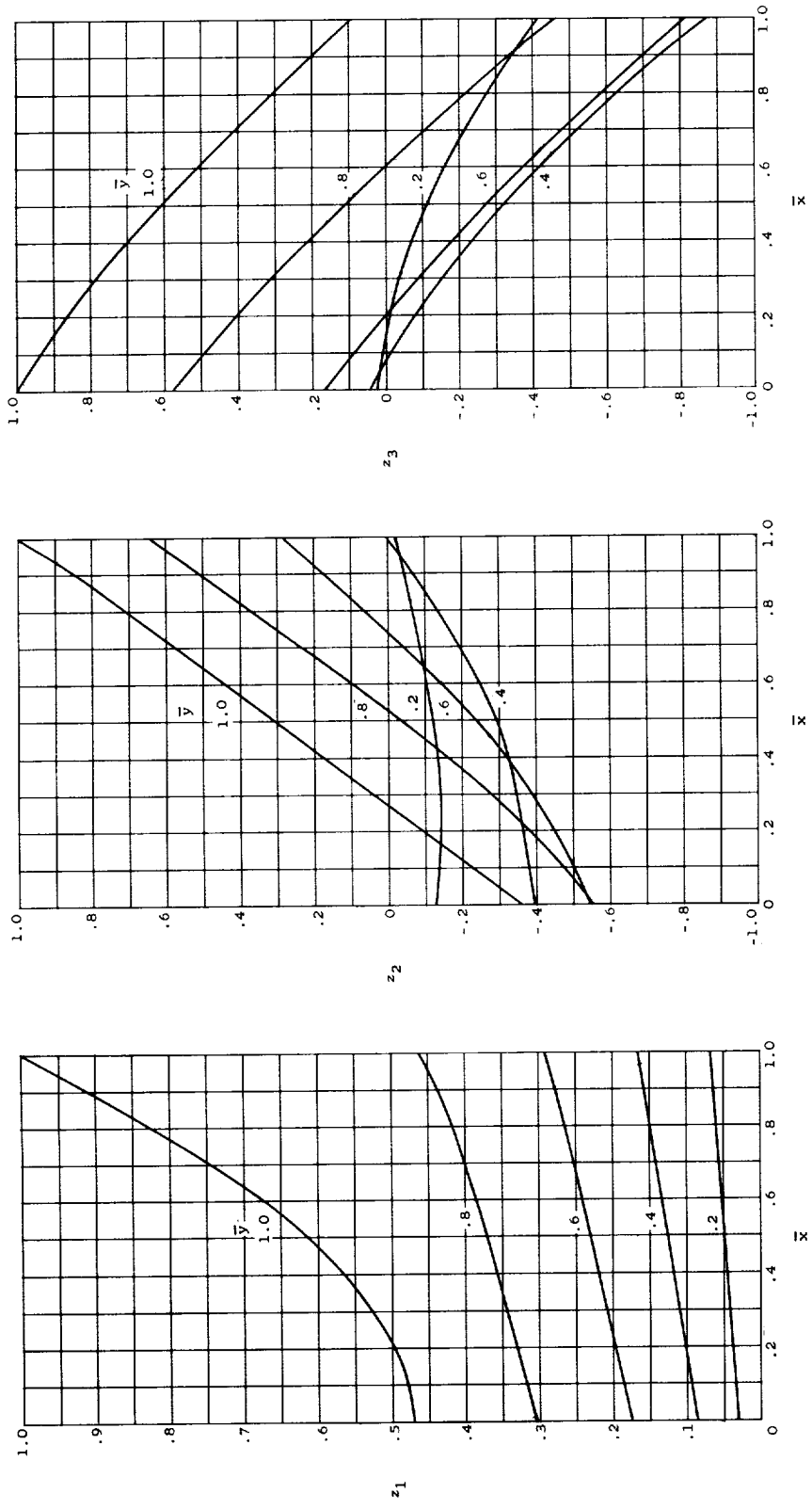

(a) Coupled modes.

Figure 3.- Vibration modes for 30° wing.

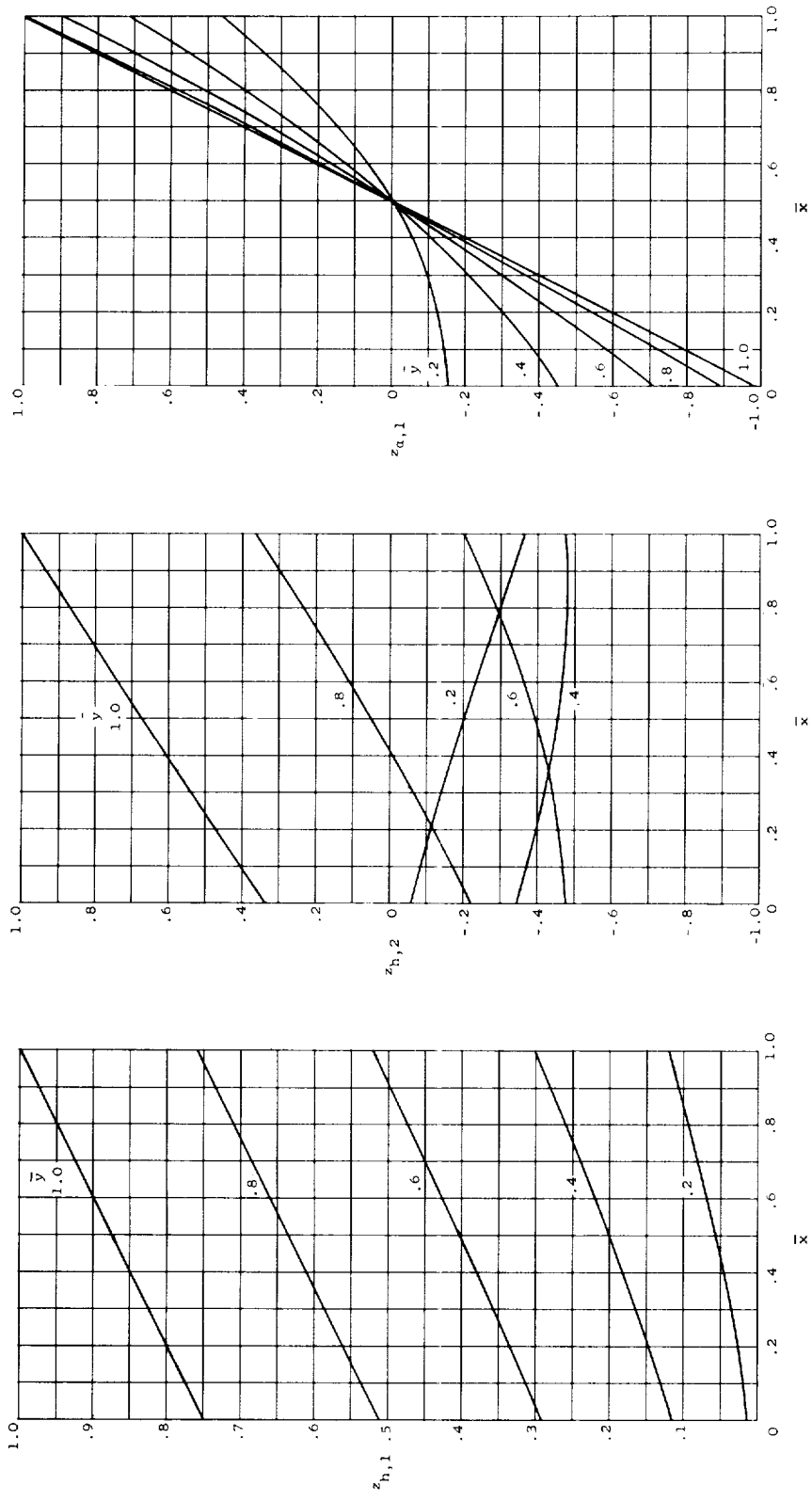

(b) Uncoupled modes.

Figure 3.- Concluded.

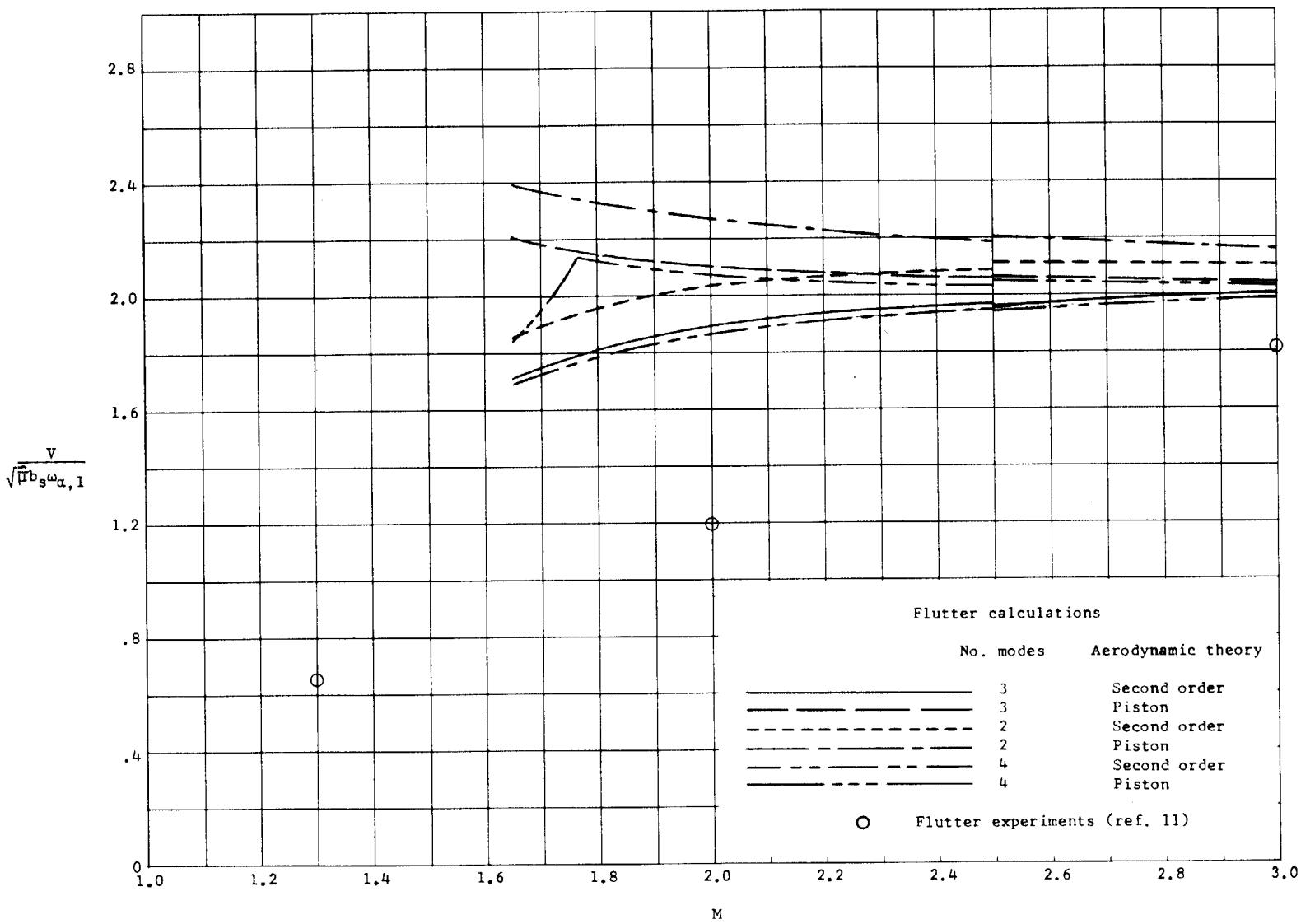

(a) Uncoupled modes.

Figure 4.- Calculated flutter-speed coefficients for 15° wing showing effects of number of vibration modes employed. All calculations include finite wing thickness and no modification of load in the tip triangle.

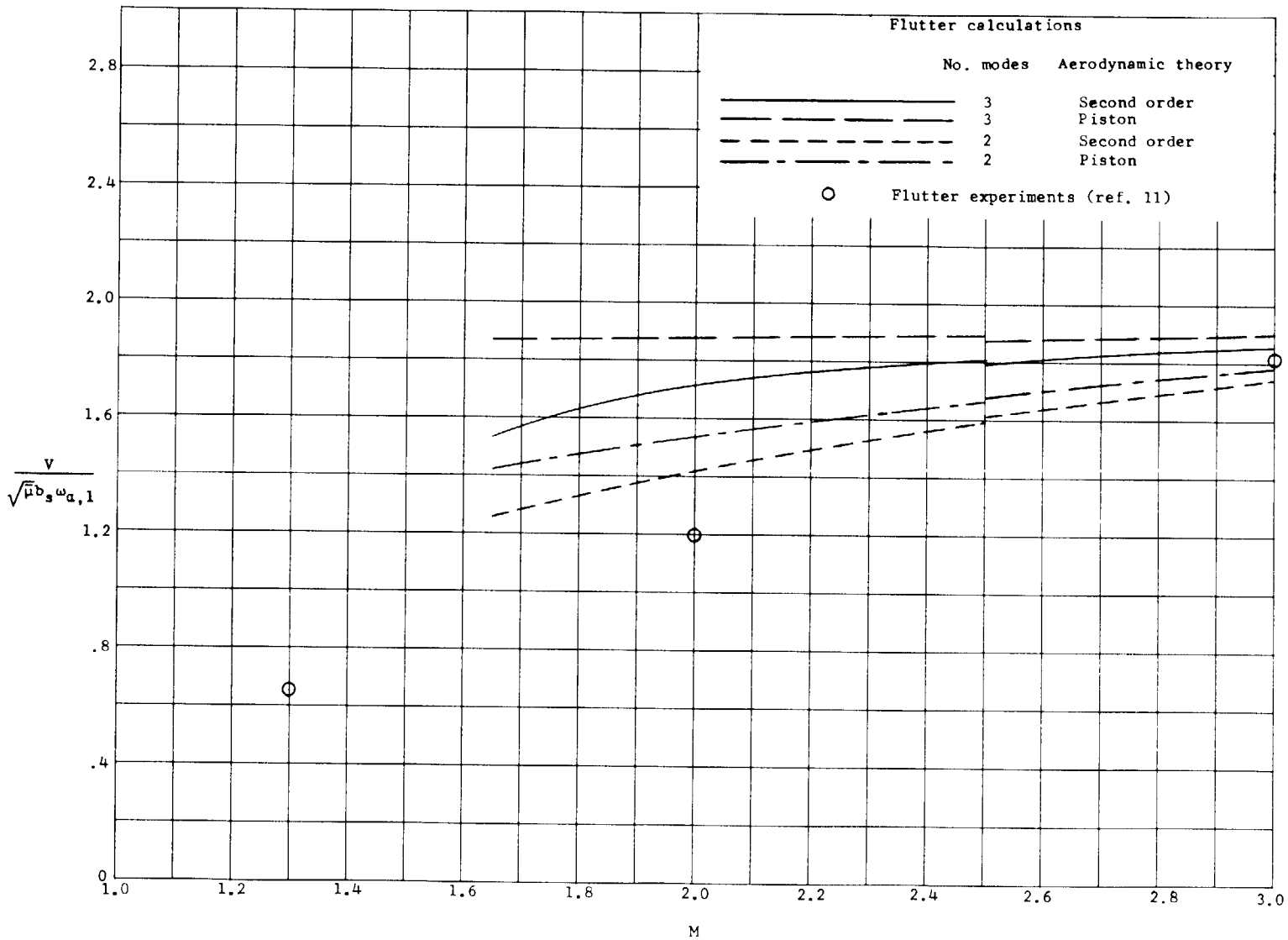

(b) Coupled modes.

Figure 4.- Concluded.

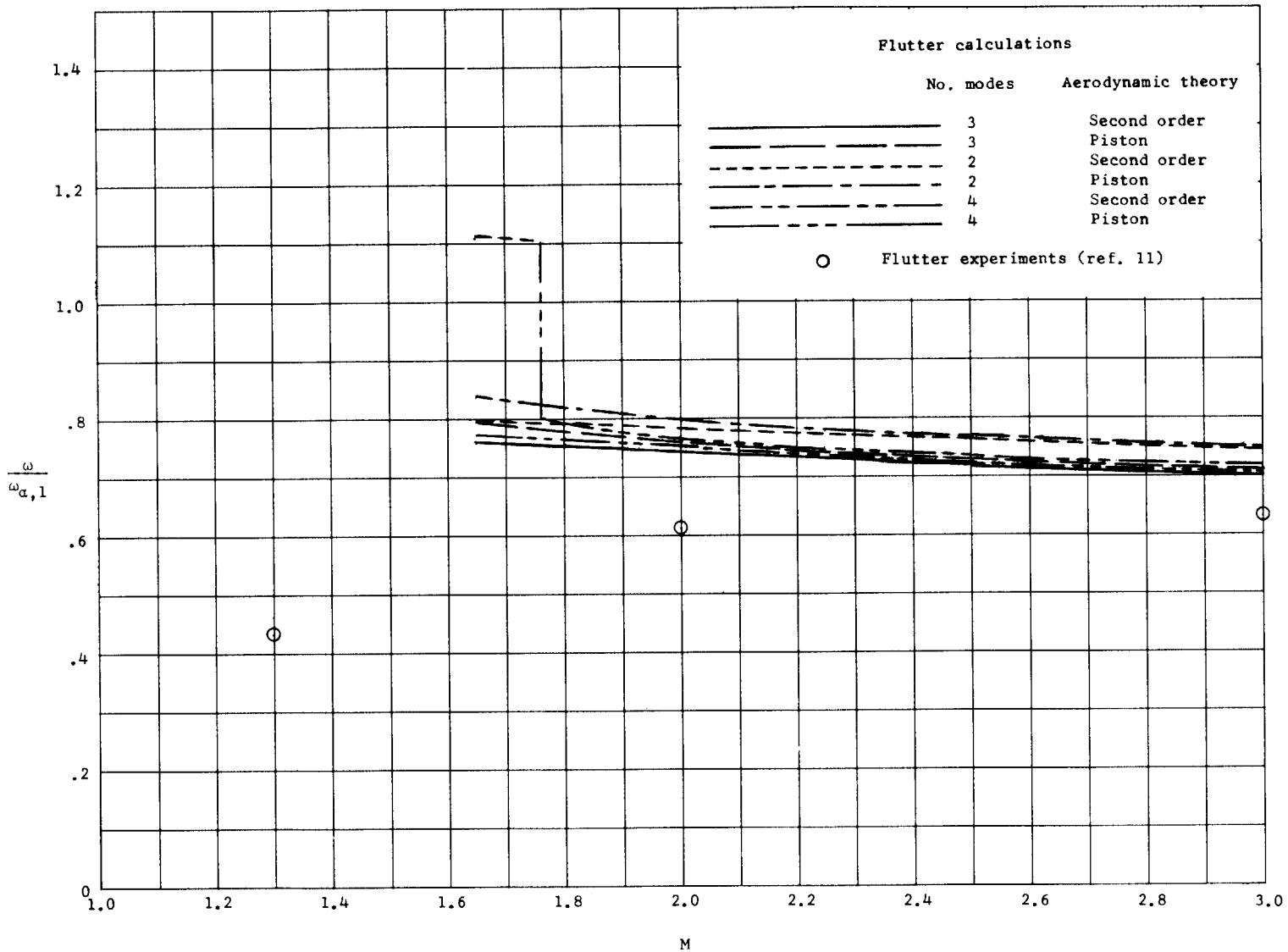

(a) Uncoupled modes.

Figure 5.- Calculated flutter-frequency ratios for 15° wing showing effects of number of modes employed. All calculations include finite wing thickness and no modification of load in tip triangle.

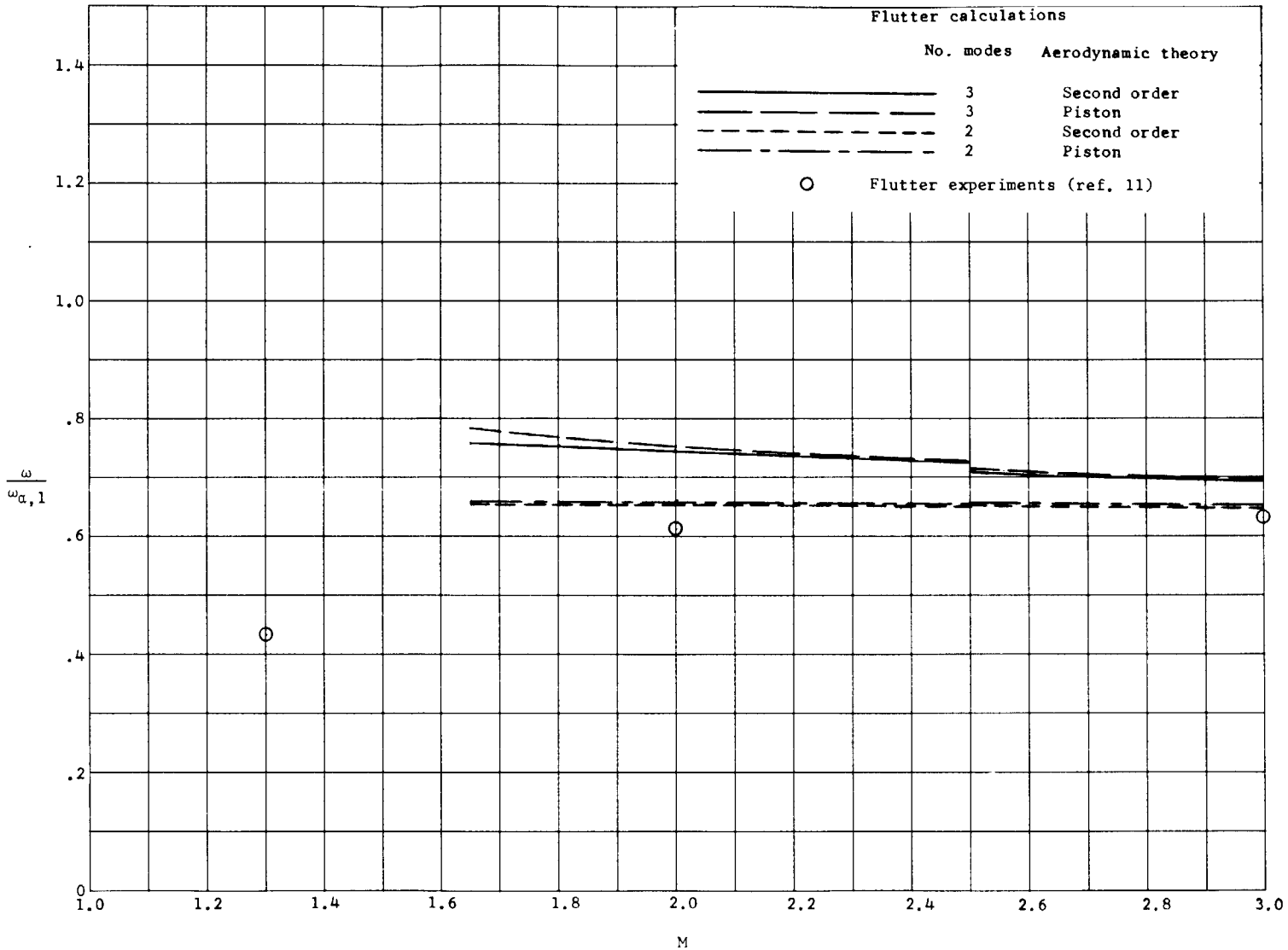

(b) Coupled modes.

Figure 5.- Concluded.

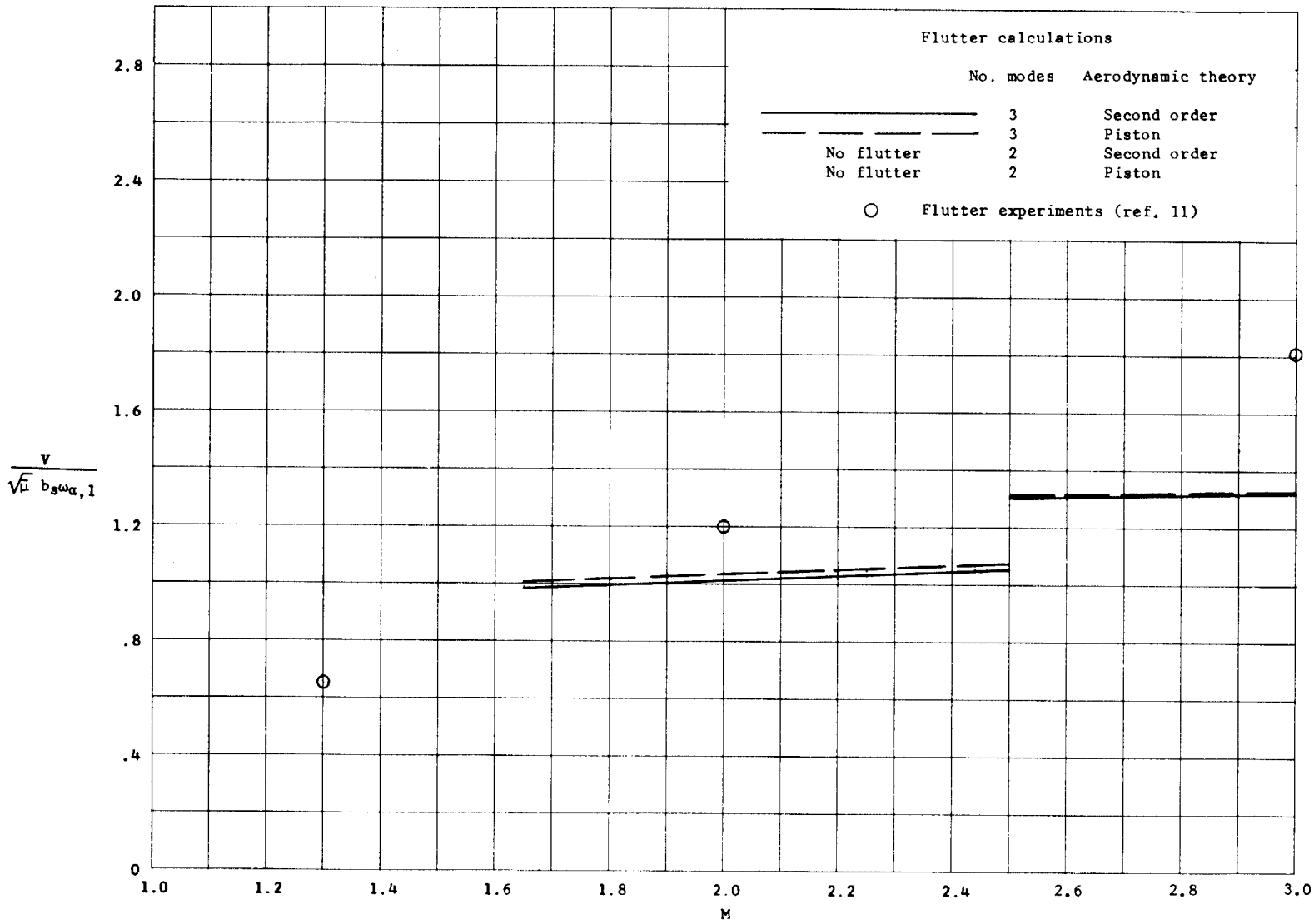

(a) Uncoupled modes.

Figure 6.- Calculated flutter-speed coefficients for 15° wing showing effects of number of vibration modes employed. All calculations neglect finite wing thickness and include no modification of load in tip triangle.

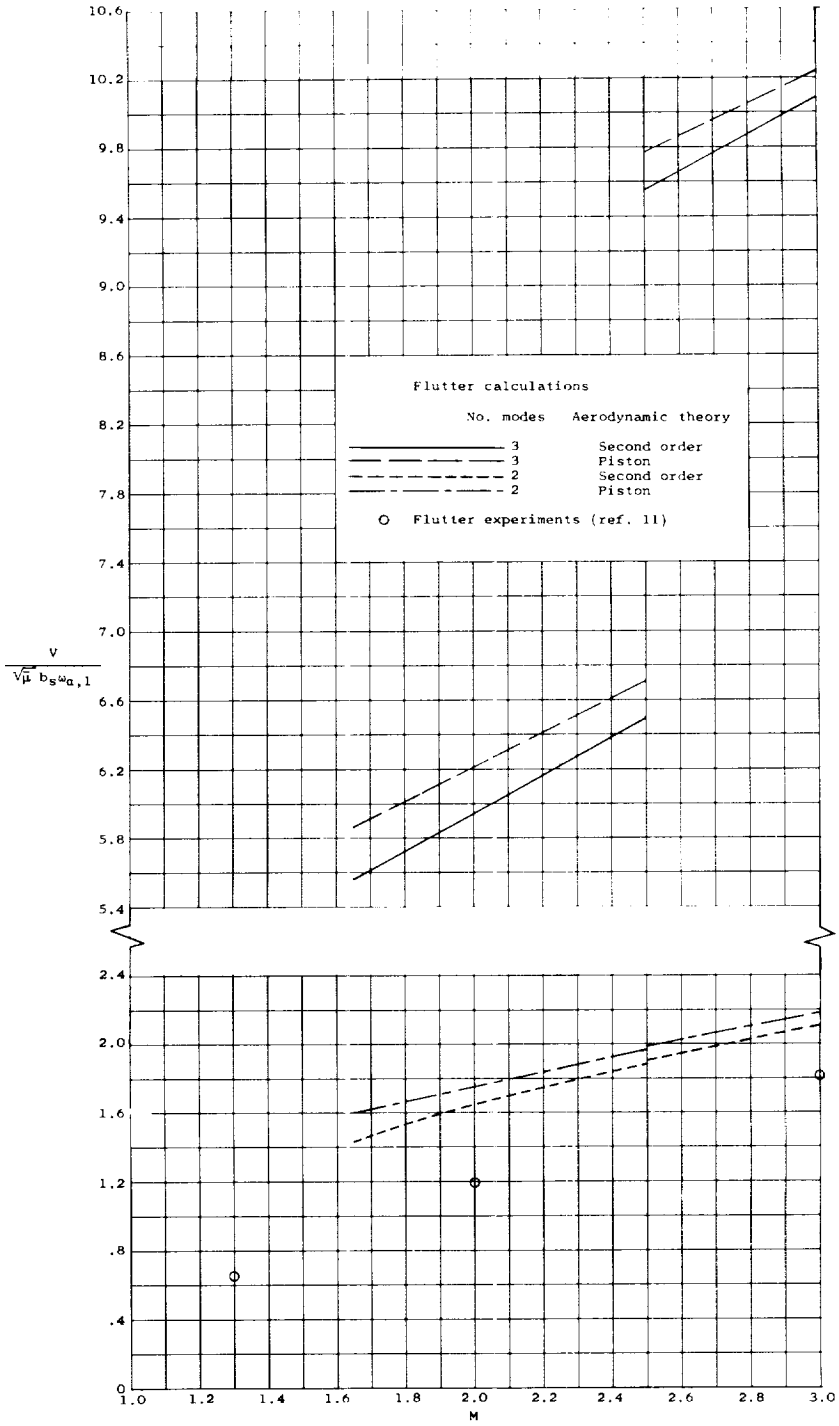

(b) Coupled modes.

Figure 6.- Concluded.

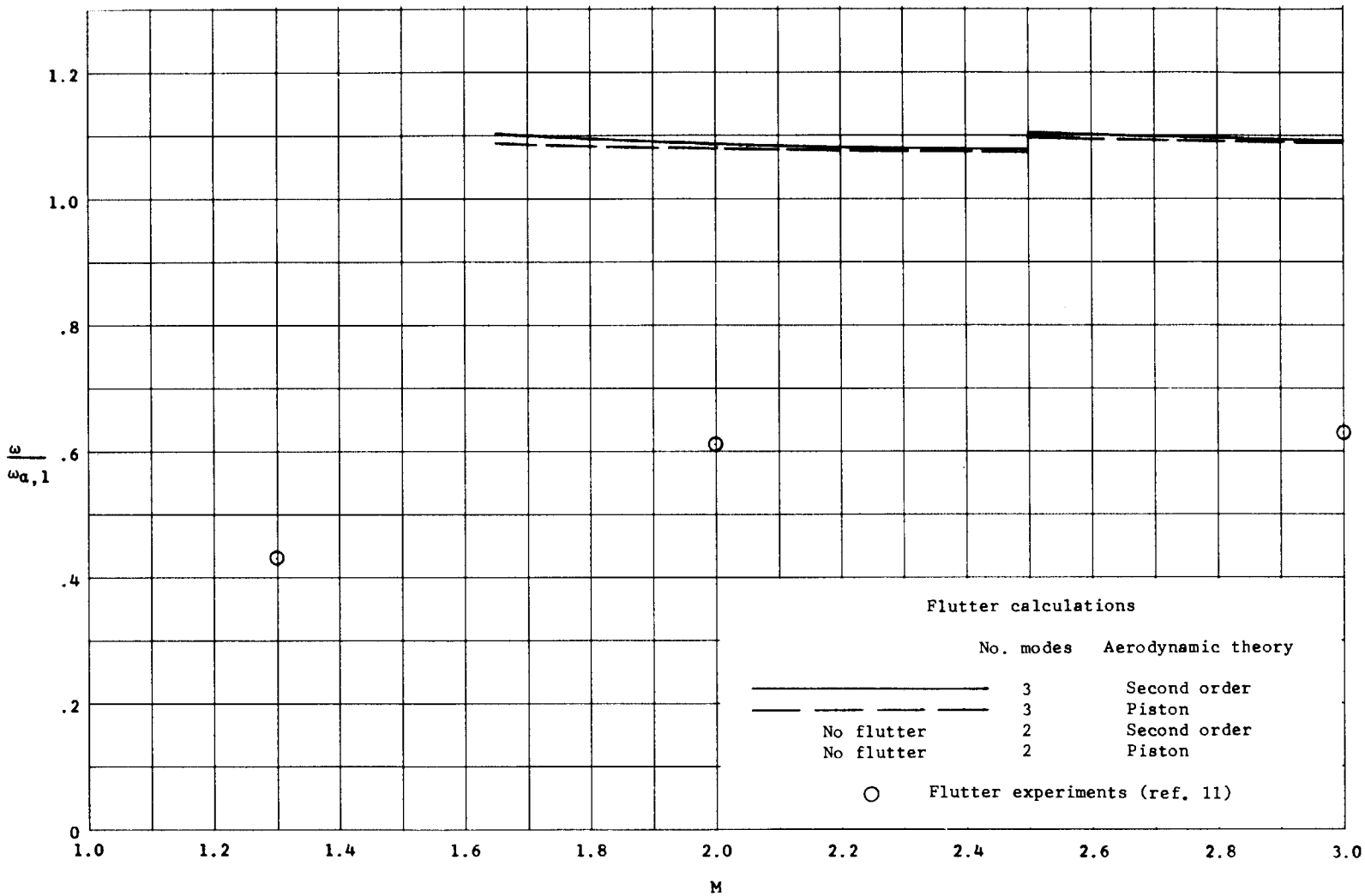

(a) Uncoupled modes.

Figure 7.- Calculated flutter-frequency ratios for 15° wing showing effects of number of modes employed. All calculations neglect finite wing thickness and include no modification of load in tip triangle.

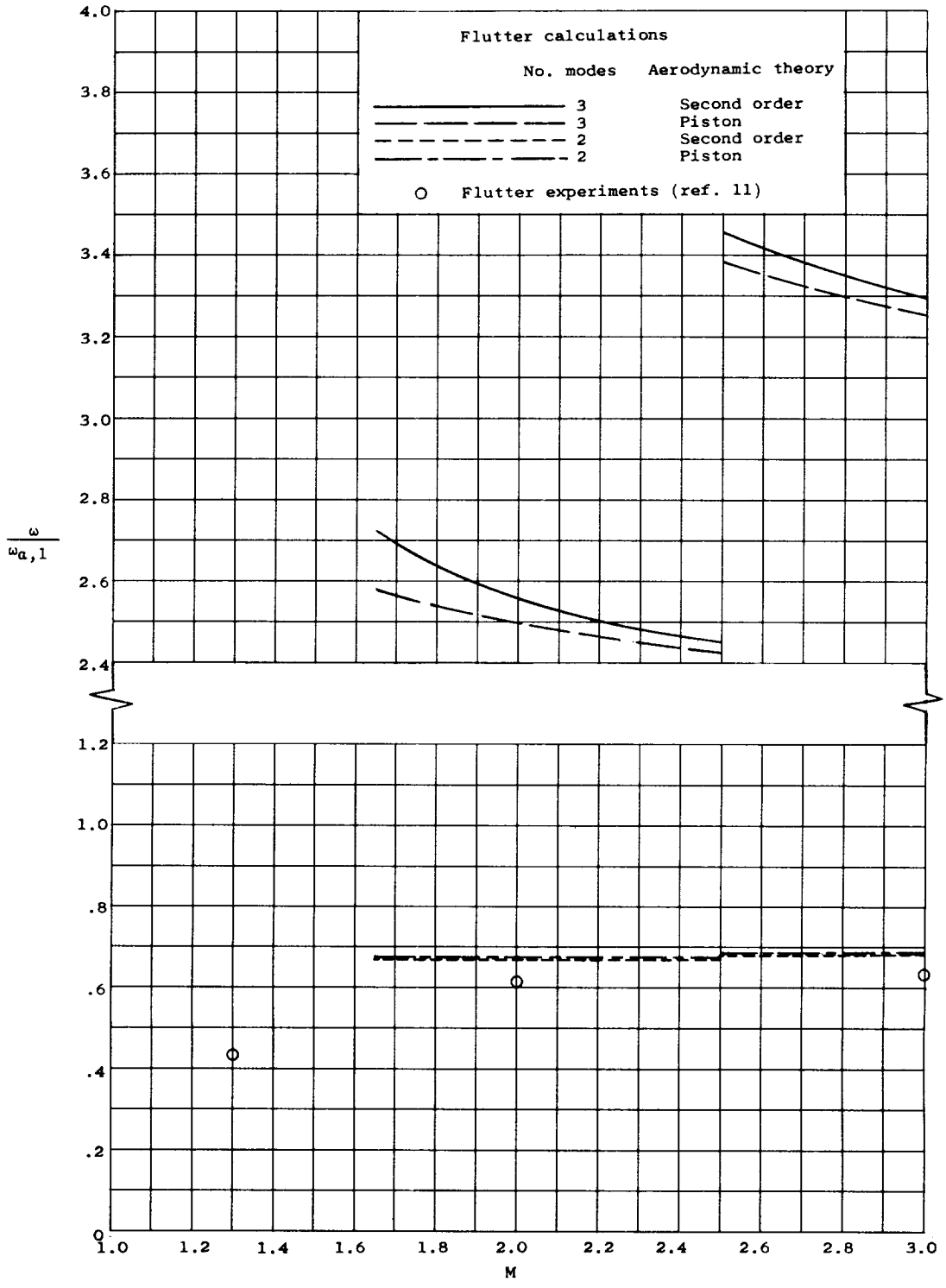

(b) Coupled modes.

Figure 7.- Concluded.

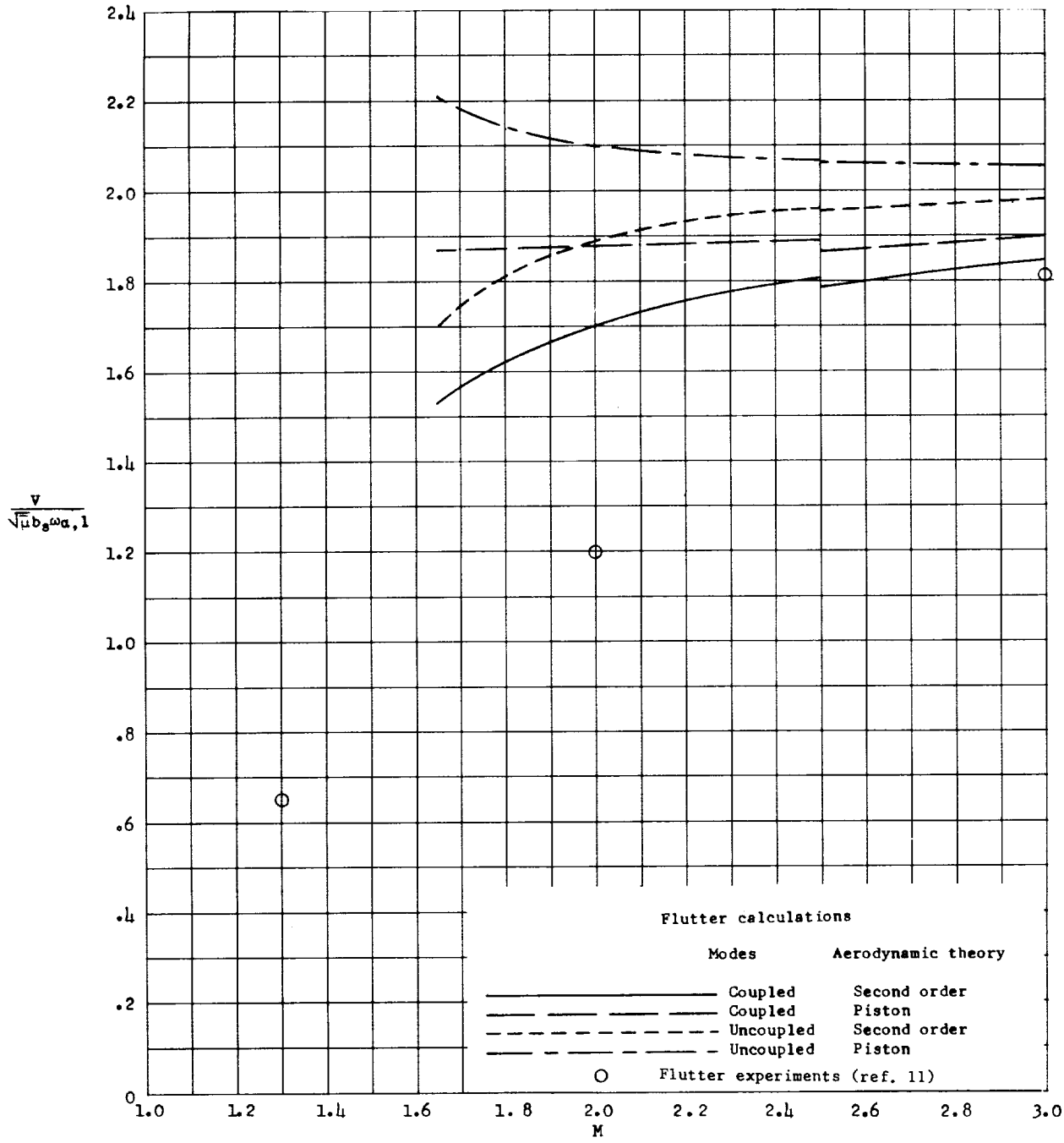

(a) No modification of load in tip triangle.

Figure 8.- Calculated flutter-speed coefficients for 15° wing with three different load representations in the tip region. All calculations include finite wing thickness and three vibration modes.

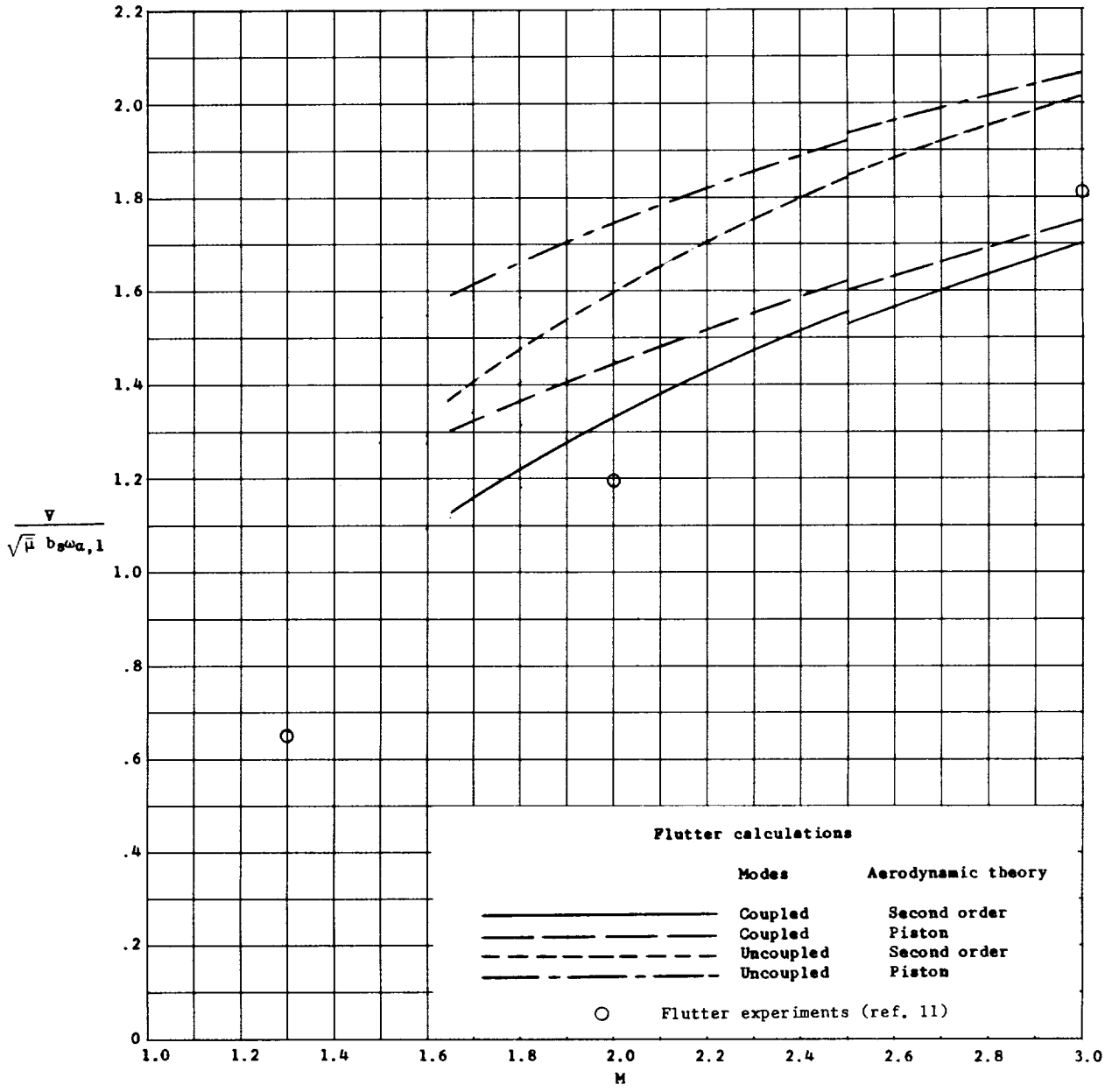

(b) Calculated modification of load in tip triangle.

Figure 8.- Continued.

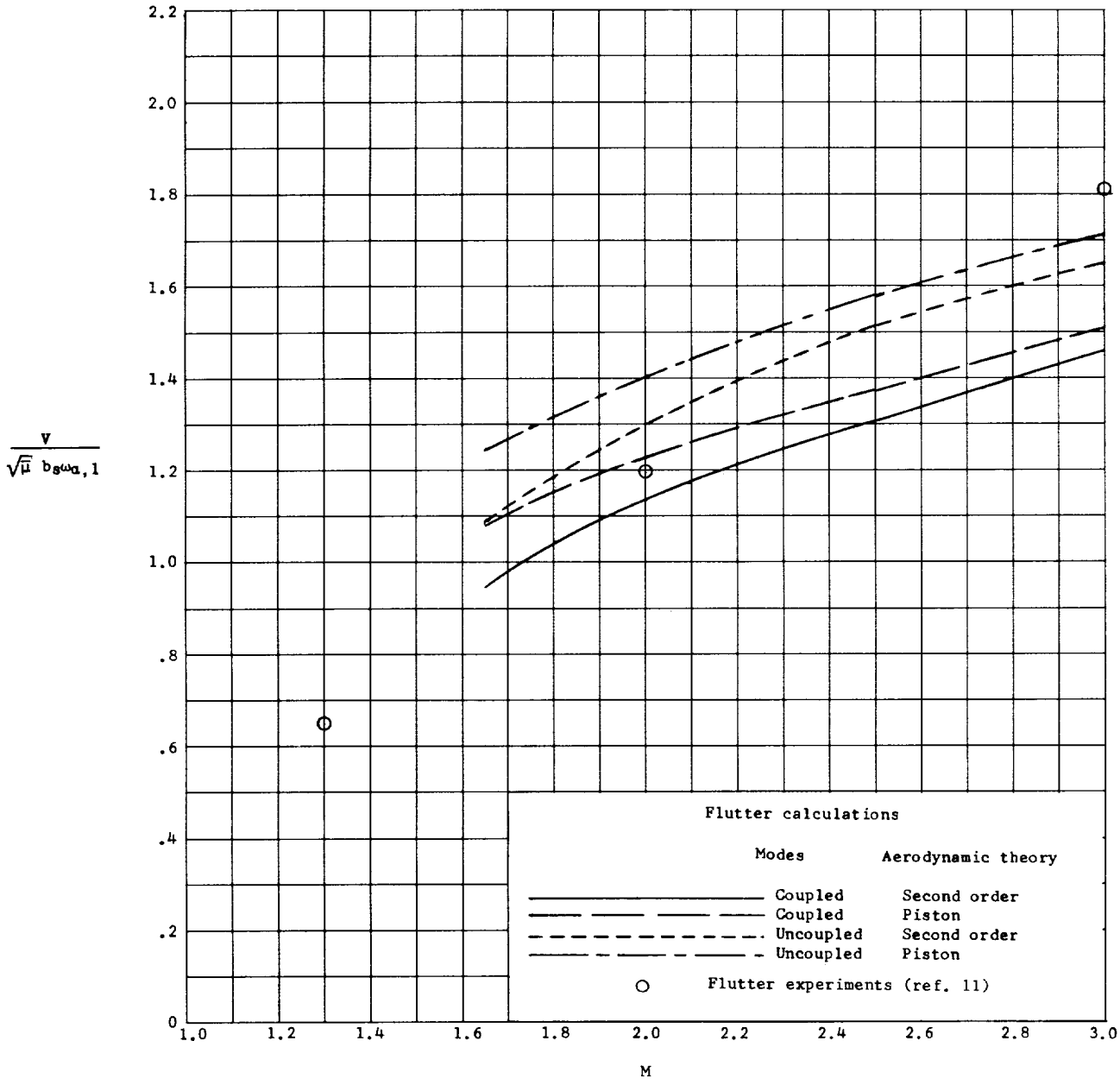

(c) Zero load in tip triangle.

Figure 8.- Concluded.

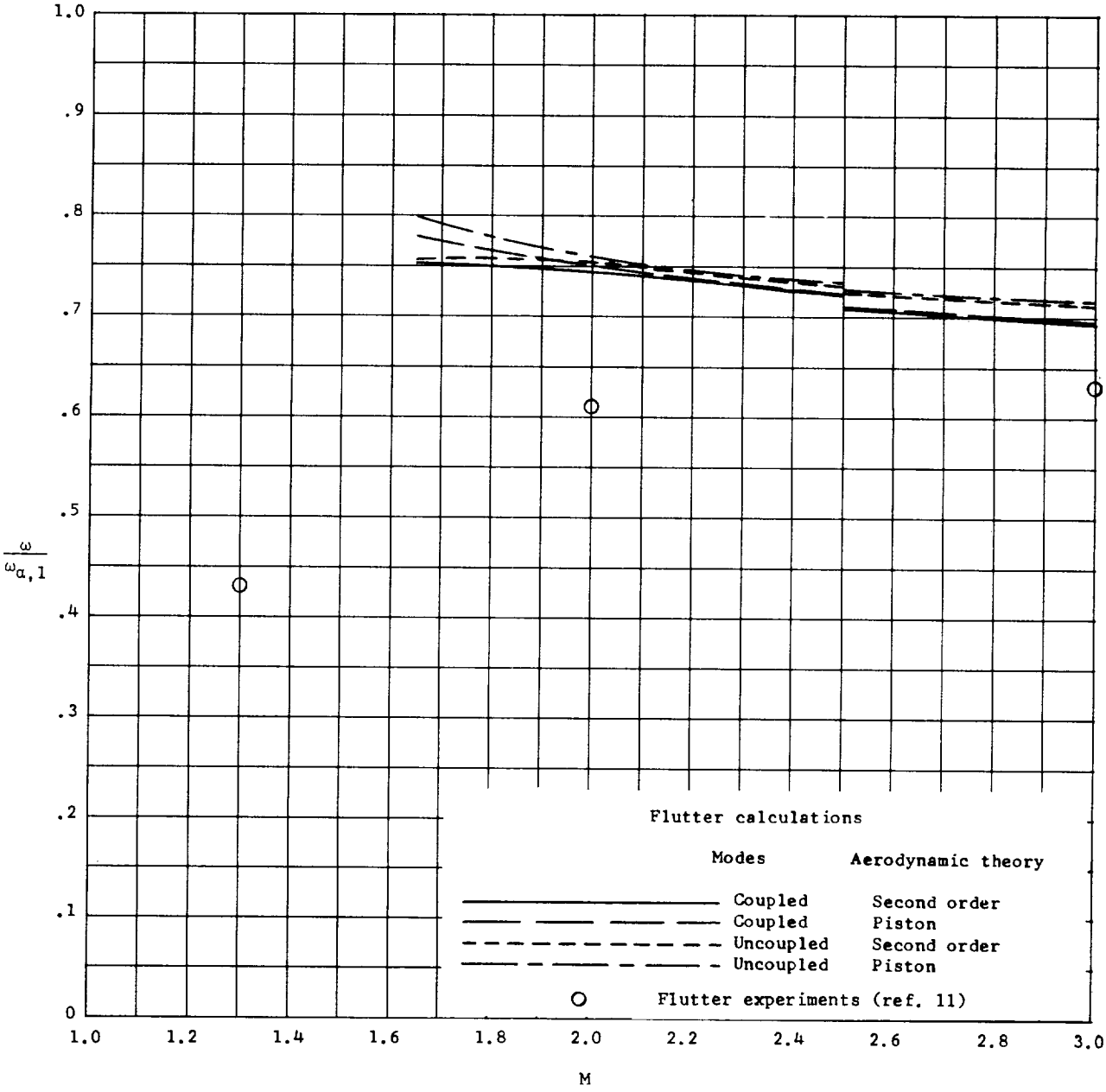

(a) No modification of load in tip triangle.

Figure 9.- Calculated flutter-frequency ratios for 15° wing with three different load representations in the tip region. All calculations include finite wing thickness and three vibration modes.

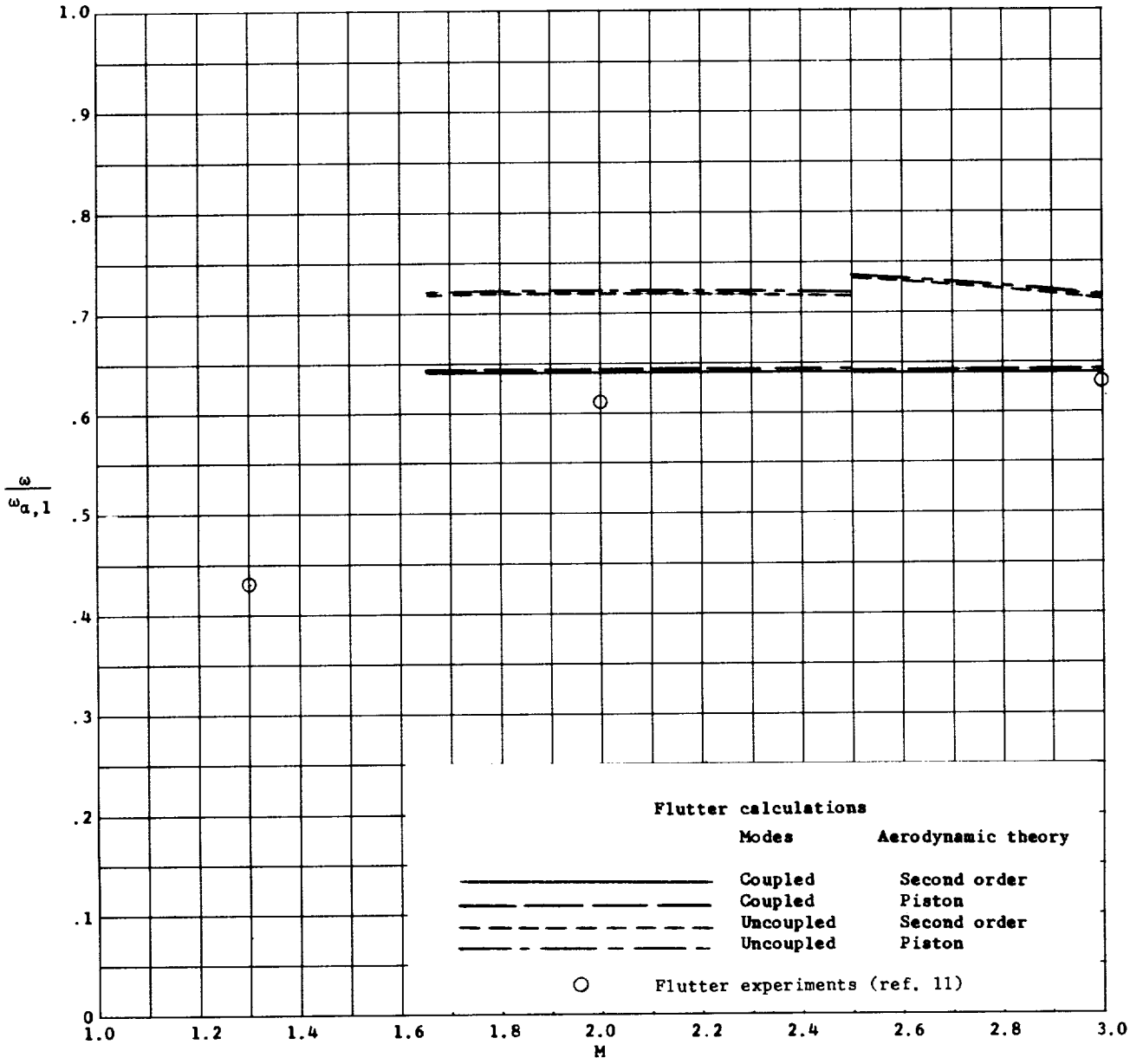

(b) Calculated modification of load in tip triangle.

Figure 9.- Continued.

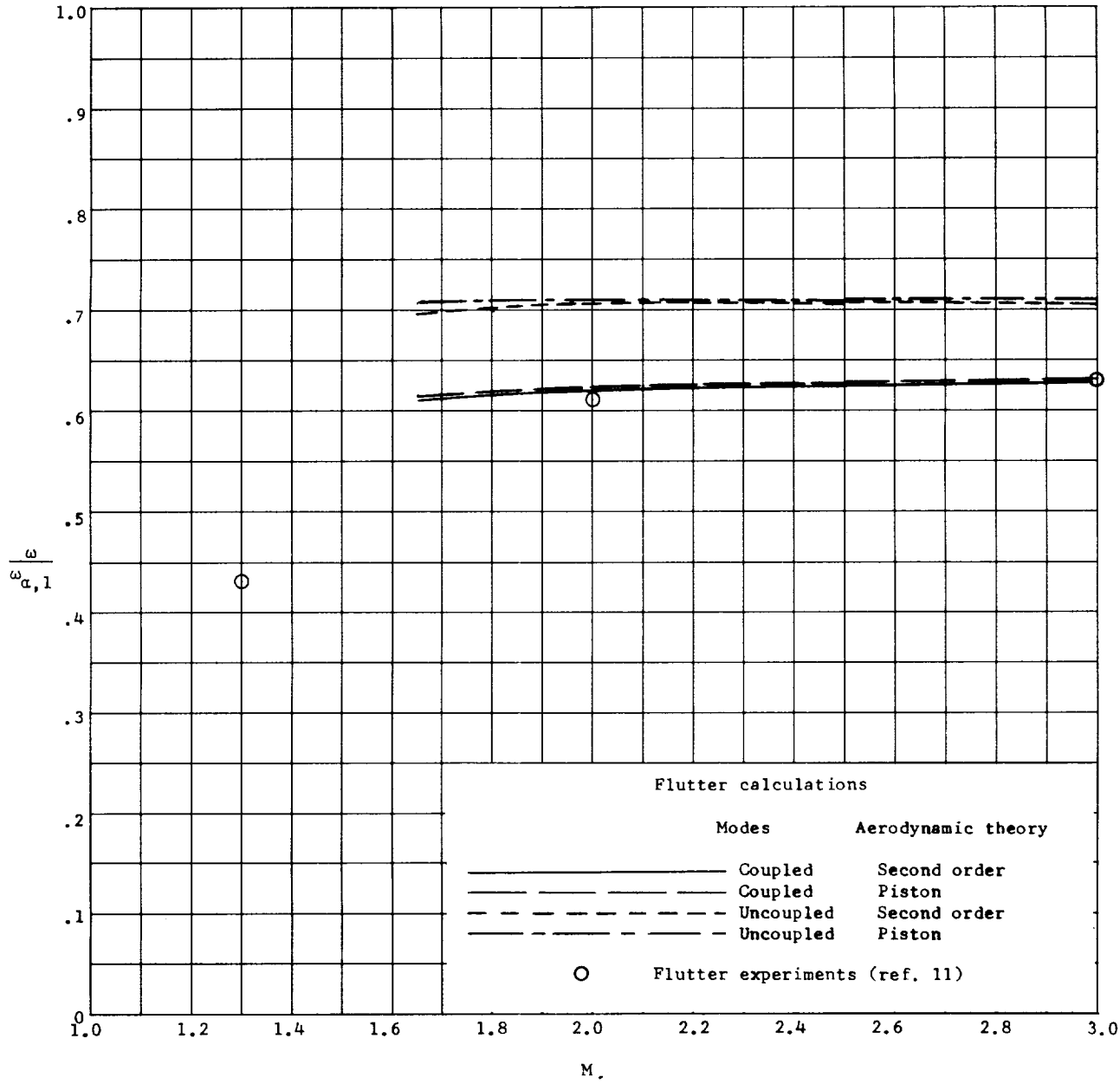

(c) Zero load in tip triangle.

Figure 9.- Concluded.

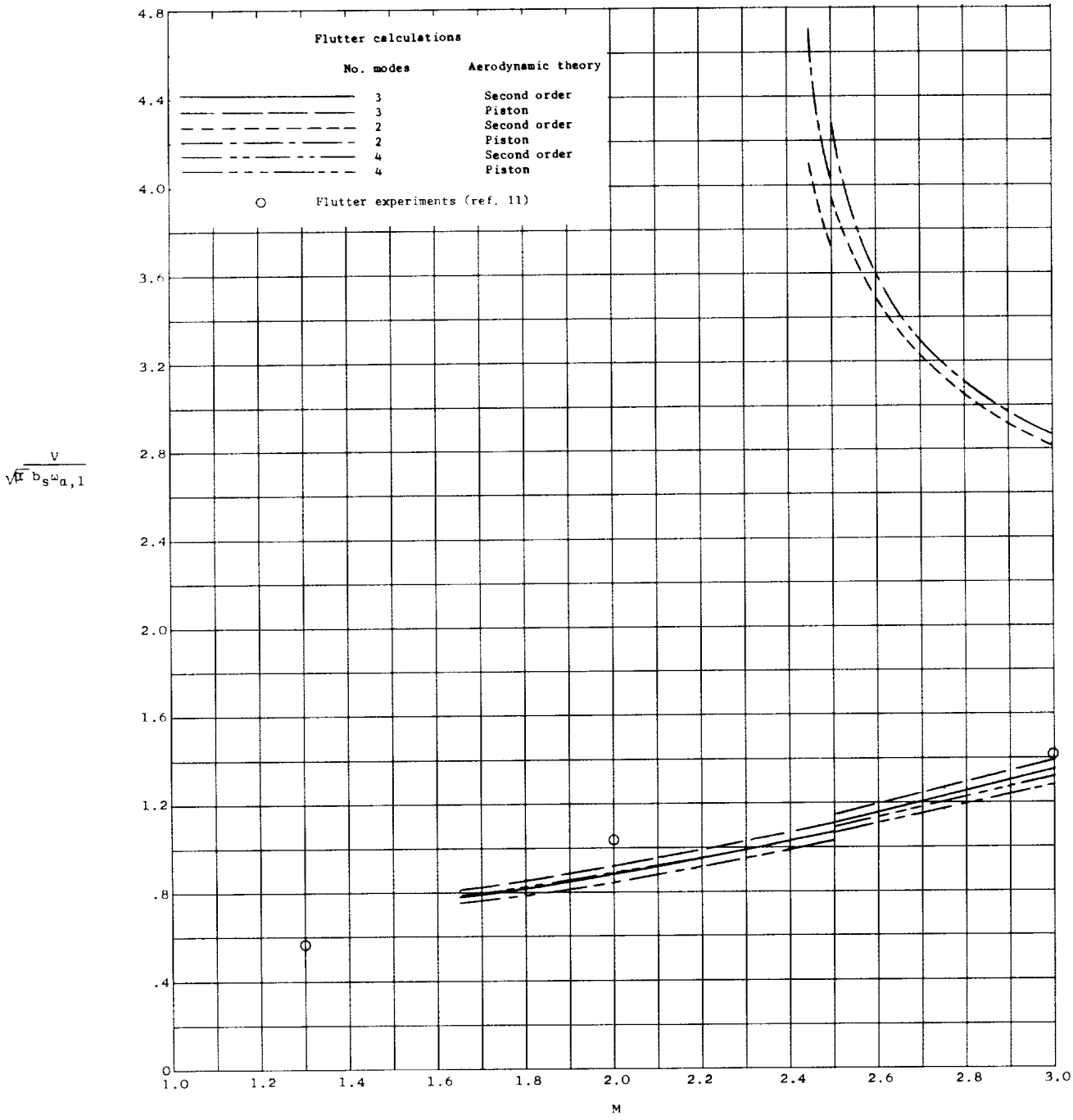

Figure 10.- Calculated flutter-speed coefficients for 30° wing showing effects of number of uncoupled vibration modes employed. All calculations include finite wing thickness and no modification of load in tip triangle.

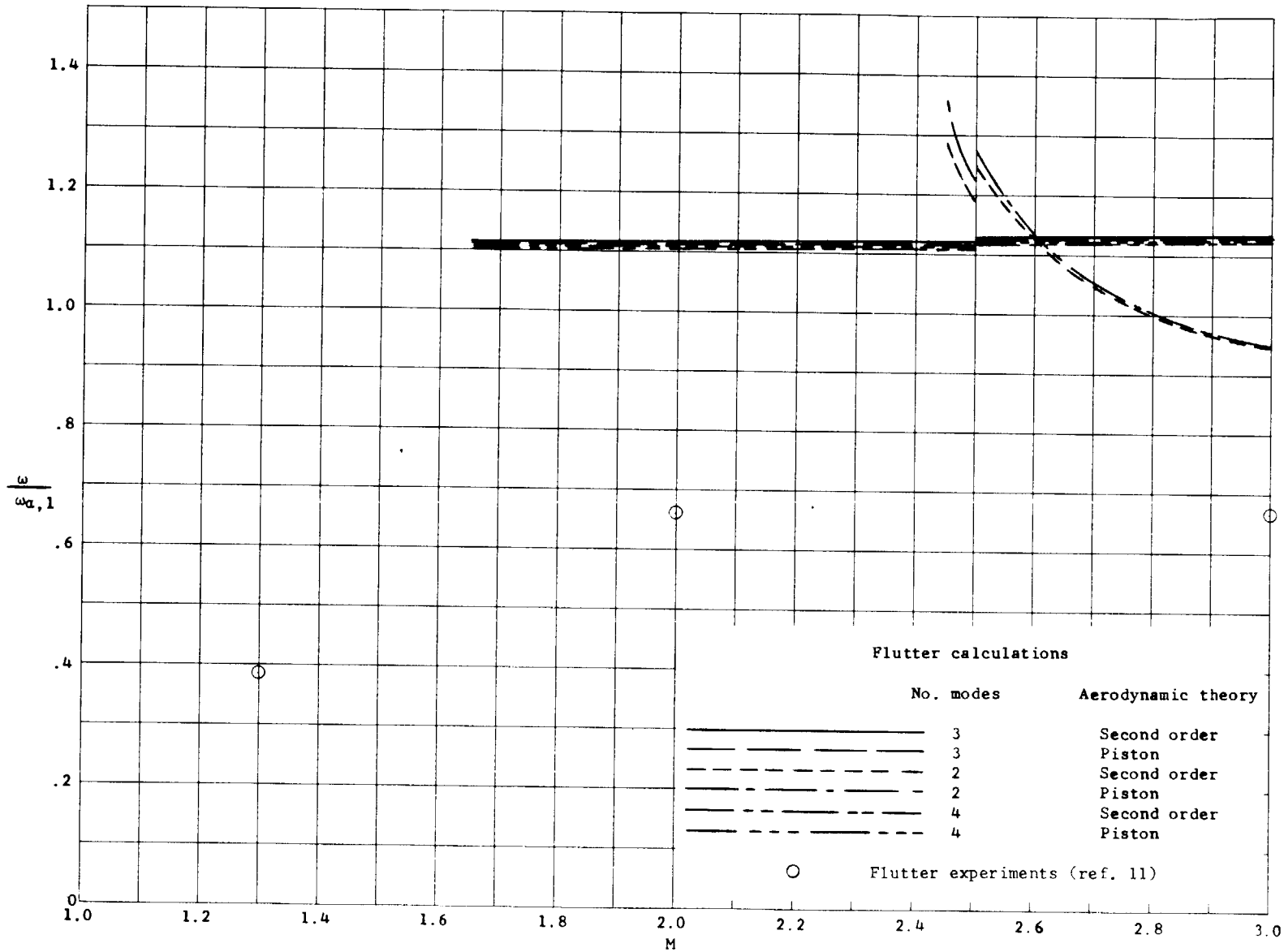

Figure 11.- Calculated flutter-frequency ratios for 30° wing showing effects of number of uncoupled vibration modes employed. All calculations include finite wing thickness and no modification of load in tip triangle.

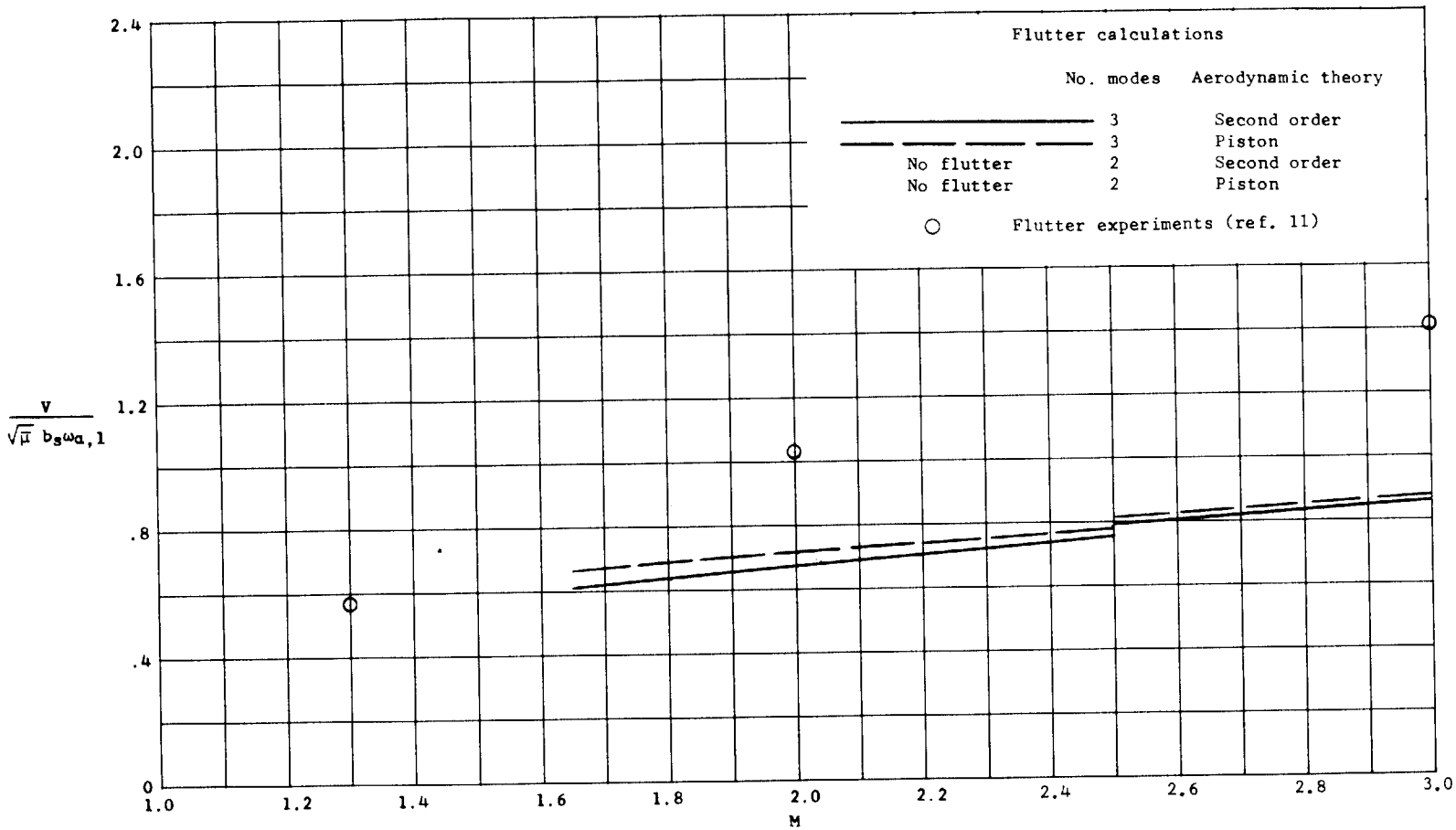

Figure 12.- Calculated flutter-speed coefficients for 30° wing with uncoupled vibration modes. These calculations neglect finite thickness and include no modification of load in tip triangle.

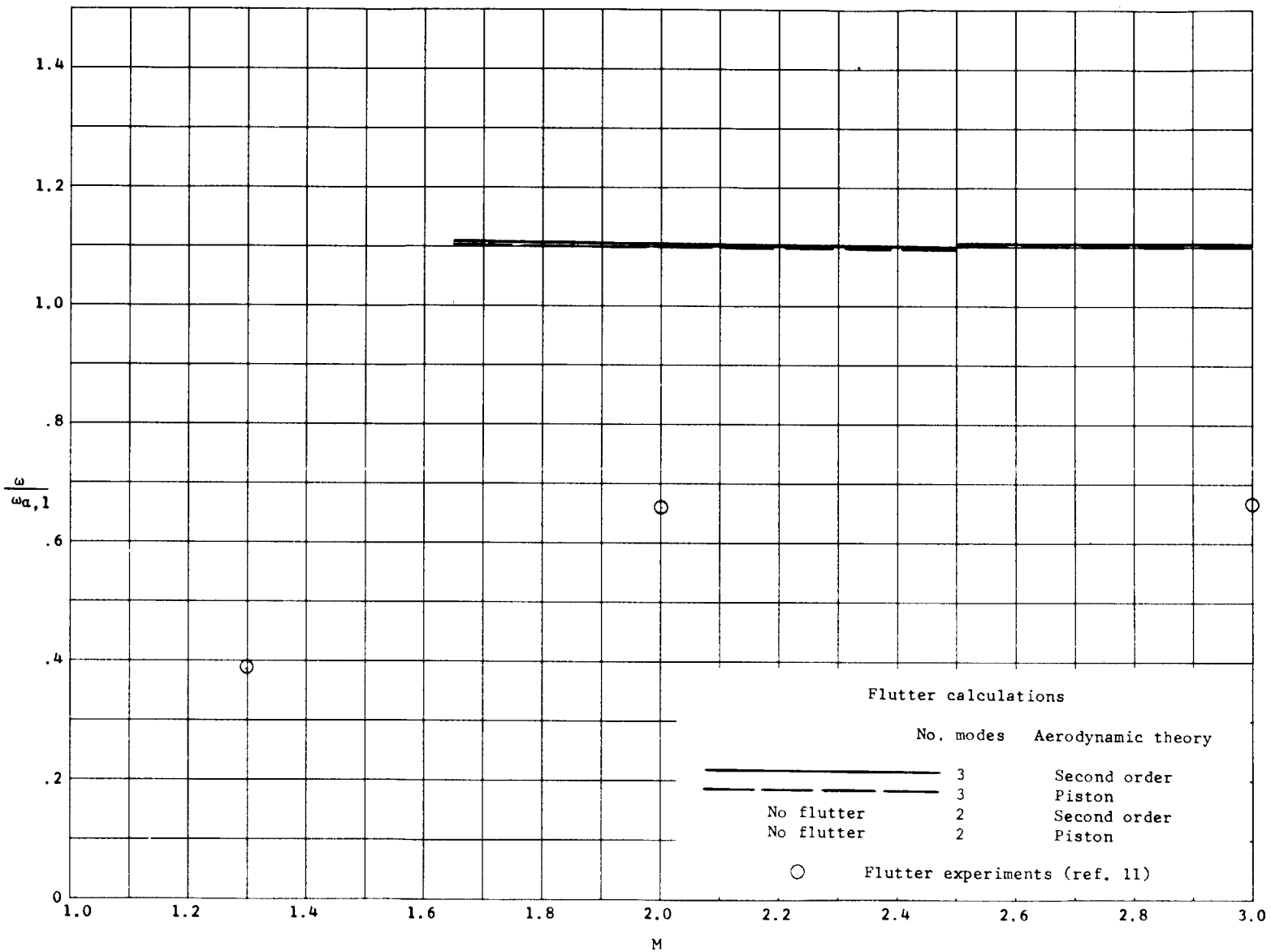

Figure 13.- Calculated flutter-frequency ratios for 30° wing with uncoupled vibration modes. These calculations neglect finite wing thickness and include no modification of load in tip triangle.

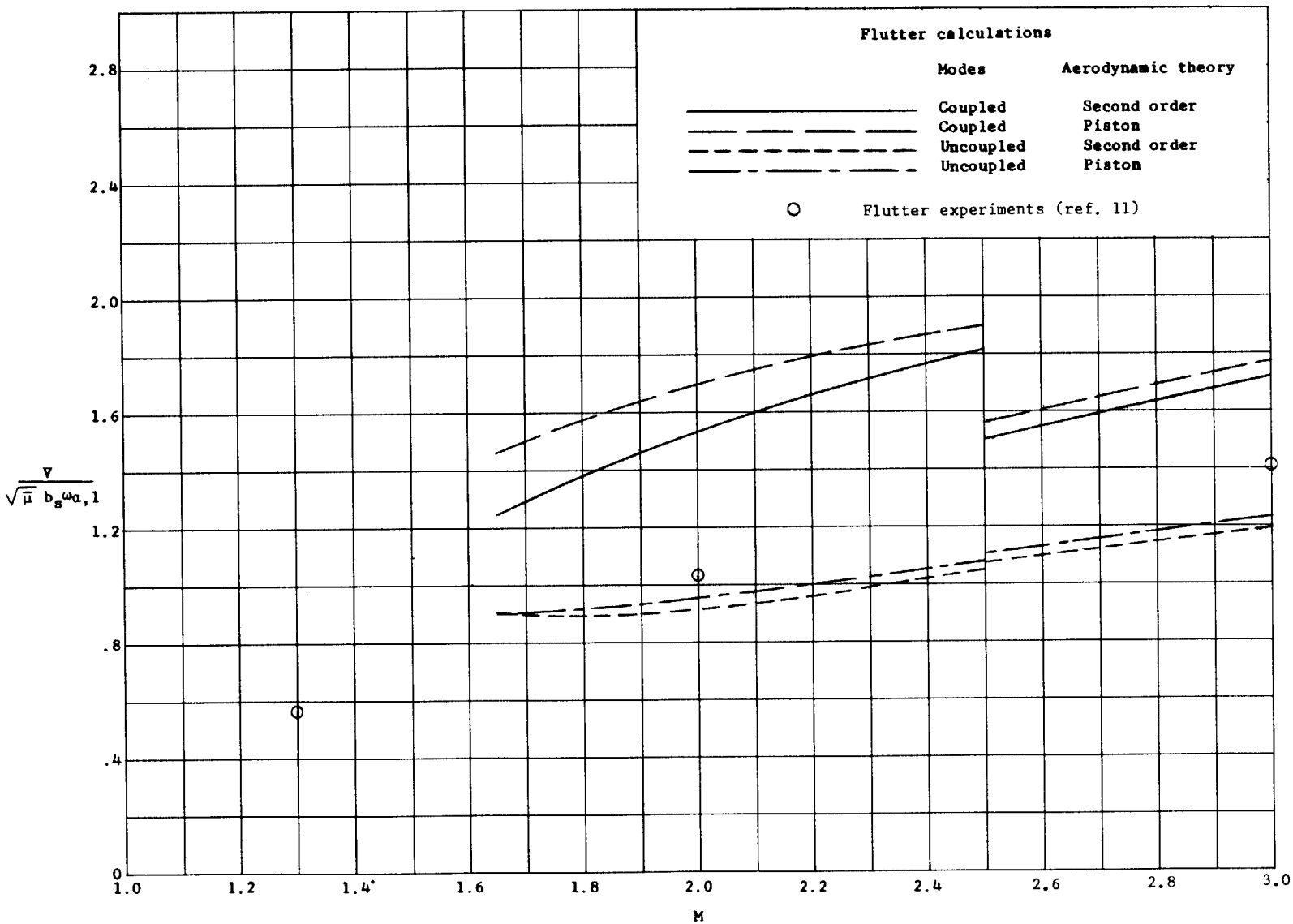

Figure 14.- Calculated flutter-speed coefficients for 30° wing. All calculations employ calculated modification of load in tip triangle, finite wing thickness, and three vibration modes.

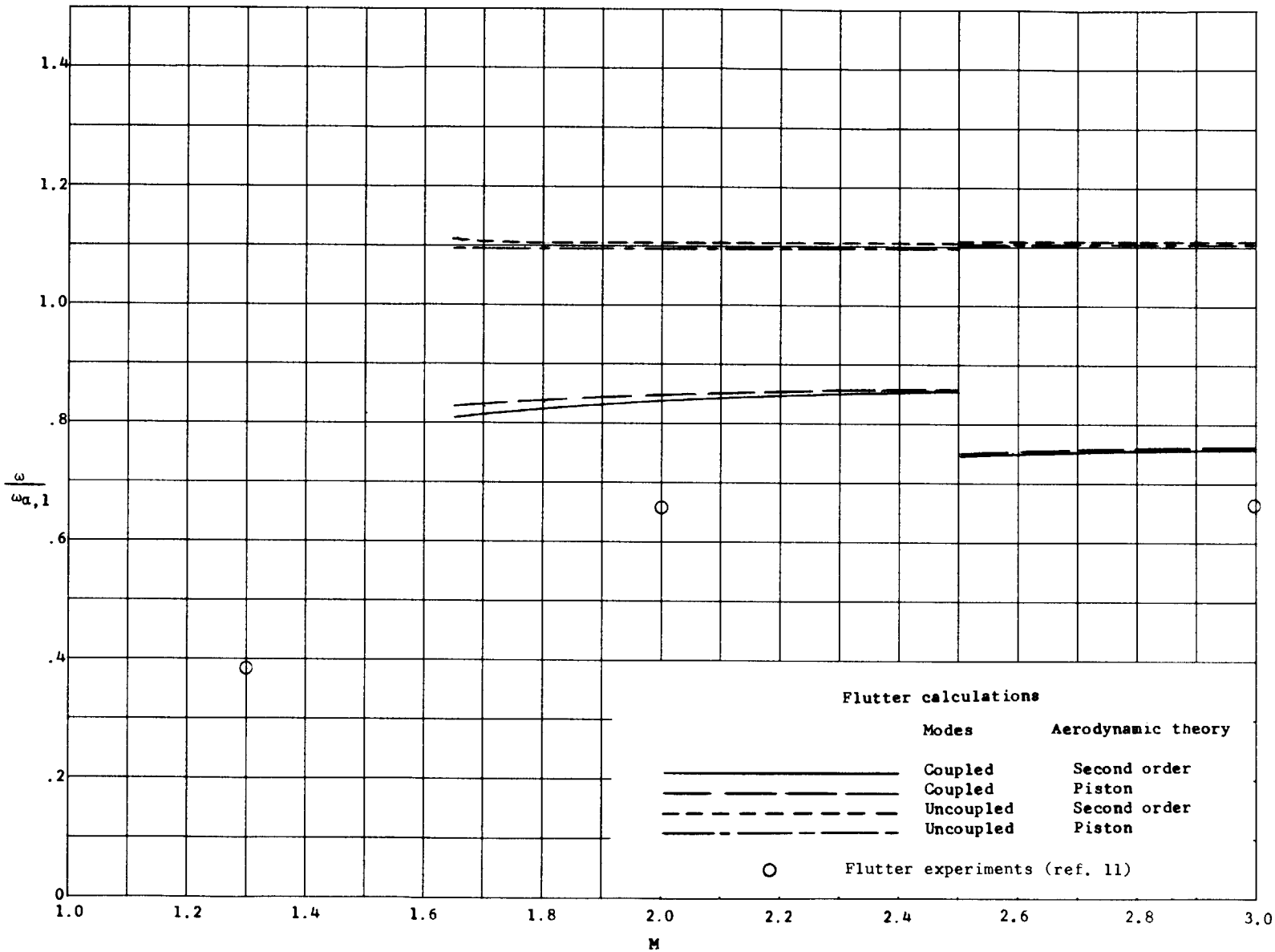

Figure 15.- Calculated flutter-frequency ratios for 30° wing. All calculations employ calculated modification of load in tip triangle, finite wing thickness, and three vibration modes.